Performance-Based Liquefaction Potential Evaluation

Steven L. Kramer

132E More Hall
University of Washington
Seattle, WA 98195-2700
206/685-2642
kramer@u.washington.edu

Roy T. Mayfield

Consulting Engineer
Kirkland, WA

Yi-Min Huang

Landau Associates
Edmonds, WA

USGS Research Award 06HQGR0041 (2/1/06 – 1/31/08)

September, 2008

Research supported by the U.S. Geological Survey (USGS), Department of the Interior, under USGS award number 06HQGR0041. The views and conclusions contained in this document are those of the authors and should not be interpreted as necessarily representing the official policies, either expressed or implied, of the U.S. Government.

Table of Contents

Chapter 1 – Introduction

Liquefaction of soil has been a topic of considerable interest to geotechnical engineers since its devastating effects were widely observed following 1964 earthquakes in Niigata, Japan and Alaska. Since that time, a great deal of research on soil liquefaction has been completed in many countries that are exposed to this important seismic hazard. This work has resulted in the development of useful empirical procedures that allow deterministic and probabilistic evaluation of liquefaction potential for a specified level of ground shaking.

In practice, the level of ground shaking is usually obtained from the results of a probabilistic seismic hazard analysis (PSHA); although that ground shaking model is determined probabilistically, a single level of ground shaking is selected and used within the liquefaction potential evaluation. In reality, though, a given site may be subjected to a wide range of ground shaking levels ranging from low levels that occur relatively frequently to very high levels that occur only rarely, each with different potential for triggering liquefaction.

This report shows how the entire range of potential ground shaking can be considered in a fully probabilistic liquefaction potential evaluation using a performance-based earthquake engineering (PBEE) framework, and how the results of that analysis can be implemented using a mapped scalar quantity. The procedure can result in a direct estimate of the return period for liquefaction, rather than a factor of safety or probability of liquefaction conditional upon ground shaking with some specified return period. As such, the performance-based approach can be considered to produce a more complete and consistent indication of the likelihood of liquefaction at a given location than conventional procedures.

The report is organized in a series of chapters that present the background material, derivation of the performance-based approach, and implementation of the performance-based approach via complete and simplified performance-based analyses. Chapter 2 presents a discussion of soil liquefaction potential and its conventional evaluation. Chapter 3 provides a general description of performance-based earthquake engineering, and a basic framework for its implementation. The complete performance-based liquefaction potential evaluation procedure is described in Chapter 4. Chapter 5 describes a simplified procedure in which mapped values of a scalar quantity can be used to closely approximate the results of a complete performance-based analysis of liquefaction potential. Chapter 6 summarizes the project and its findings, and presents conclusions that can be drawn from them.

Chapter 2 – Liquefaction Potential

Soil liquefaction has been a problem of great interest to geotechnical engineers for nearly 50 years, ever since its damaging effects were so extensively observed following earthquakes in Alaska and Japan in 1964. Since that time, research on soil liquefaction has led to a sound understanding of the basic mechanics of liquefiable soils, and to practical procedures for evaluation of liquefaction hazards.

Liquefaction hazard evaluations generally deal with three issues – liquefaction susceptibility, initiation of liquefaction, and effects of liquefaction. The issues are generally addressed in the order listed, since the latter issues are dependent on the former. Assuming a soil is judged to be susceptible to liquefaction, its potential for initiation under the anticipated earthquake loading conditions is then judged. This process is usually described as an evaluation of the soil's "liquefaction potential."

2.1 Evaluation of Liquefaction Potential

Liquefaction potential is generally evaluated by comparing consistent measures of earthquake loading and liquefaction resistance. It has become common to base the comparison on cyclic shear stress amplitude, usually normalized by initial vertical effective stress and expressed in the form of a cyclic stress ratio, *CSR*, for loading and a cyclic resistance ratio, *CRR*, for resistance. The potential for liquefaction is then described in terms of a factor of safety against liquefaction, $FS_L = CRR/CSR$. If the factor of safety is less than one, i.e., if the loading exceeds the resistance, liquefaction is expected to be triggered.

2.1.1 Characterization of Earthquake Loading

The cyclic stress ratio is most commonly evaluated using the "simplified method" first described by Seed and Idriss (1971), which can be expressed as

$$CSR = 0.65 \frac{a_{max}}{g} \cdot \frac{\sigma_{vo}}{\sigma'_{vo}} \cdot \frac{r_d}{MSF} \tag{2.1}$$

where a_{max} = peak ground surface acceleration, g = acceleration of gravity (in same units as a_{max}), σ_{vo} = initial vertical total stress, σ'_{vo} = initial vertical effective stress, r_d = depth reduction factor, and MSF = magnitude scaling factor, which is a function of earthquake magnitude. The depth reduction factor accounts for compliance of a typical soil profile and the magnitude scaling factor acts as a proxy for the number of significant cycles, which is related to the ground motion duration. It should be noted that two pieces of loading information – a_{max} and earthquake magnitude – are required for estimation of the cyclic stress ratio.

2.1.2 Characterization of Liquefaction Resistance

The cyclic resistance ratio is generally obtained by correlation to insitu test results, usually standard penetration (SPT), cone penetration (CPT), or shear wave velocity (V_s) tests. Of these, the SPT has been most commonly used and will be used in the remainder of this paper. A number of SPT-based procedures for deterministic (Seed and Idriss, 1971; Seed et al., 1984; Youd et al., 2001, Idriss and Boulanger, 2004) and probabilistic (Liao et al., 1988; Toprak et al., 1999; Youd and Noble, 1997; Juang and Jiang, 2000; Cetin et al., 2004) estimation of liquefaction resistance have been proposed.

2.1.2.1 Deterministic Approach

Figure 2.1(a) illustrates the widely used liquefaction resistance curves recommended by Youd et al. (2001), which are based on discussions at a NCEER Workshop (National Center for Earthquake Engineering Research, 1997). The liquefaction evaluation procedure described by Youd et al. (2001) will be referred to hereafter as the NCEER procedure. The NCEER procedure has been shown to produce reasonable predictions of liquefaction potential (i.e., few cases of non-prediction for sites at which liquefaction was observed) in past earthquakes, and is widely used in contemporary geotechnical engineering practice. For the purposes of this paper, a conventionally liquefaction-resistant site will be considered to be one for which $FS_L \geq 1.2$ for a 475-yr ground motion using the NCEER procedure. This standard is consistent with that recommended by Martin and Lew (1999), for example, and is considered representative of those commonly used in current practice.

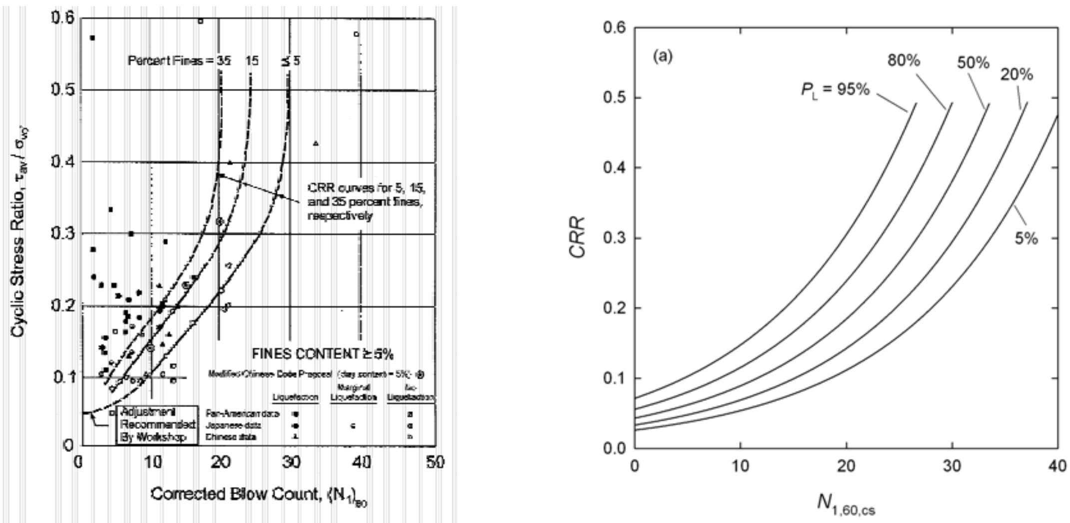

Figure 2.1. (a) Deterministic cyclic resistance curves proposed by Youd et al. (2001), and (b) cyclic resistance curves of constant probability of liquefaction with measurement/estimation errors by Cetin et al., (2004).

2.1.2.2 Probabilistic Approach

Recently, a detailed review and careful re-interpretation of liquefaction case histories (Cetin, 2000; Cetin et al., 2004) was used to develop new probabilistic procedures for evaluation of liquefaction potential. The probabilistic implementation of the Cetin et al. (2004) procedure produces a probability of liquefaction, P_L, which can be expressed as

$$P_L = \Phi\left[-\frac{(N_1)_{60}(1+\theta_1 FC)-\theta_2 \ln CSR_{eq} - \theta_3 \ln M_w - \theta_4 \ln\left(\sigma_{vo}'/p_a\right)+\theta_5 FC+\theta_6}{\sigma_\varepsilon}\right] \tag{2.2}$$

where Φ is the standard normal cumulative distribution function, $(N_1)_{60}$ = corrected SPT resistance, FC = fines content (in percent), CSR_{eq} = cyclic stress ratio (Equation 2.1) without MSF, M_w = moment magnitude, σ'_{vo} = initial vertical effective stress, p_a is atmospheric pressure (in same units as σ'_{vo}), σ_ε is a measure of the estimated model and parameter uncertainty, and θ_1-θ_6 are model coefficients obtained by regression. As Equation (2.2) shows, the probability of liquefaction includes both loading terms (again, peak acceleration, as reflected in the cyclic stress ratio, and magnitude) and resistance terms (SPT resistance, fines content, and vertical effective stress). Mean values of the model coefficients are presented for two conditions in Table 2.1 – a case in which the uncertainty includes parameter measurement/estimation errors and a case in which the effects of measurement/estimation errors have been removed. The former would correspond to uncertainties that exist for a site investigated with a normal level of detail and the latter to a "perfect" investigation (i.e. no uncertainty in any of the variables on the right side of Equation 2.2). Figure 2.1(b) shows contours of equal P_L for conditions in which measurement/estimation errors are included; the measurement/estimation errors have only a slight influence on the model coefficients but a significant effect on the uncertainty term, σ_ε.

Table 2.1. Cetin et al. (2004) model coefficients with and without measurement/estimation errors (after Cetin et al., 2002).

Case	Measurement/estimation errors	θ_1	θ_2	θ_3	θ_4	θ_5	θ_6	σ_ε
I	Included	0.004	13.79	29.06	3.82	0.06	15.25	4.21
II	Removed	0.004	13.32	29.53	3.70	0.05	16.85	2.70

Direct comparison of the procedures described by Youd et al. (2001) and Cetin et al. (2004) is difficult because various aspects of the procedures are different. For example, Cetin et al (2004) found that the average effective stress for their critical layers were at lower effective stresses (~0.65 atm) instead of the standard 1 atm, and made allowances for those differences. Also, the basic shapes of the cyclic resistance curves are different – the Cetin et al. (2004) curves (Figure 2.1b) have a smoothly changing curvature while the Youd et al. (2001) curve (Figure 2.1a) is nearly linear at intermediate SPT resistances ($(N_1)_{60} \approx$ 10-22) with higher curvatures at lower and higher SPT resistances. An approximate comparison of the two methods can be made by substituting CRR for CSR_{eq} in Equation 2.2 and then rearranging the equation in the form

$$CRR = \exp\left[\frac{(N_1)_{60}(1+\theta_1 FC) - \theta_3 \ln M_w - \theta_4 \ln\left(\sigma'_{vo}/p_a\right) + \theta_5 FC + \theta_6 + \sigma_\varepsilon \Phi^{-1}(P_L)}{\theta_2}\right] \quad (2.3)$$

where Φ^{-1} is the inverse standard normal cumulative distribution function. The resulting value of CRR can then be used in the common expression for FS_L. Arango et al. (2004) used this formulation without measurement/estimation errors (Case II in Table 2.1) and found that the Cetin et al. (2004) and NCEER procedures yielded similar values of FS_L for a site in San

Francisco when a value of $P_L \approx 0.65$ was used in Equation (2.3). A similar exercise for a site in Seattle with measurement/estimation errors (Case I in Table 2.1) shows equivalence of FS_L when a value of $P_L \approx 0.6$ is used. Cetin et al. (2001) suggest use of a deterministic curve equivalent to that given by Equation (2.3) with $P_L = 0.15$, which would produce a more conservative result than the NCEER procedure. The differences between the two procedures are most pronounced at high *CRR* values; the NCEER procedure contains an implicit assumption of $(N_1)_{60} = 30$ as an upper bound to liquefaction susceptibility while Cetin et al. (2004), whose database contained considerably more cases at high *CSR* levels, indicate that liquefaction is possible (albeit with limited potential effects) at $(N_1)_{60}$ values above 30.

Chapter 3 – Performance-Based Earthquake Engineering

In recent years, a new paradigm referred to as performance-based earthquake engineering (PBEE) has been developed. PBEE seeks to evaluate and predict seismic performance, using the inter-related expertise, of earth scientists, engineers, and loss analysts, in terms that are useful to a diverse group of stakeholders. The roots of performance-based liquefaction assessment are in the method of seismic risk analysis introduced by Cornell (1968).

Seismic Hazard Analysis

Ground shaking levels used in seismic design and hazard evaluations are generally determined by means of seismic hazard analyses. Deterministic seismic hazard analyses are used most often for special structures or for estimation of upper bound ground shaking levels. In the majority of cases, however, ground shaking levels are determined by probabilistic seismic hazard analyses.

Probabilistic seismic hazard analyses consider the potential levels of ground shaking from all combinations of magnitude and distance for all known sources capable of producing significant shaking at a site of interest. The distributions of magnitude and distance, and of ground shaking level conditional upon magnitude and distance, are combined in a way that allows estimation of the mean annual rate at which a particular level of ground shaking will be exceeded. The mean annual rate of exceeding a ground motion parameter value, y^*, is usually expressed as λ_{y^*}; the reciprocal of the mean annual rate of exceedance is commonly referred to as the return period. The results of a PSHA are typically presented in the form of a seismic hazard curve, which graphically illustrates the relationship between λ_{y^*} and y^*.

The ground motion level associated with a particular return period is therefore influenced by contributions from a number of different magnitudes, distances, and conditional exceedance probability levels (usually expressed in terms of a parameter, ε, defined as the number of standard deviations by which $\ln y^*$ exceeds the natural logarithm of the median value of y for a given M and R). The relative contributions of each M - R pair to λ_{y^*} can be quantified by means of a deaggregation analysis (McGuire, 1995); the deaggregated contributions of magnitude and distance are frequently illustrated in diagrams such as that shown in Figure 3.1. Because both peak acceleration and magnitude are required for cyclic stress-based evaluations of liquefaction potential, the marginal distribution of magnitude can be obtained by summing the contributions of each distance and ε value for each magnitude; magnitude distributions for six return periods at a site in Seattle analyzed by the U.S. Geological Survey (http://eqhazmaps.usgs.gov) are shown in Figure 3.2. The decreasing significance of lower magnitude earthquakes for longer return periods, evident in Figure 3.2, is a characteristic shared by many other locations.

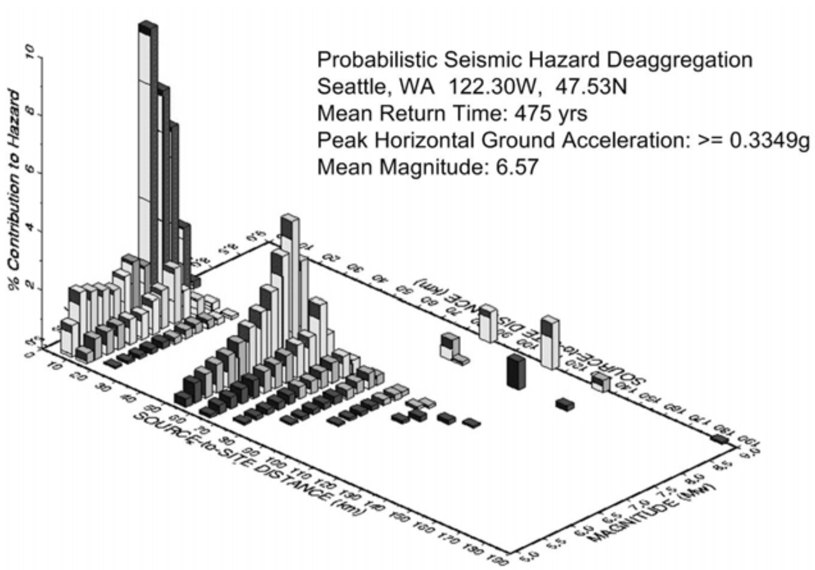

Figure 3.1. Magnitude and distance deaggregation of 475-yr peak acceleration hazard for site in Seattle, Washington.

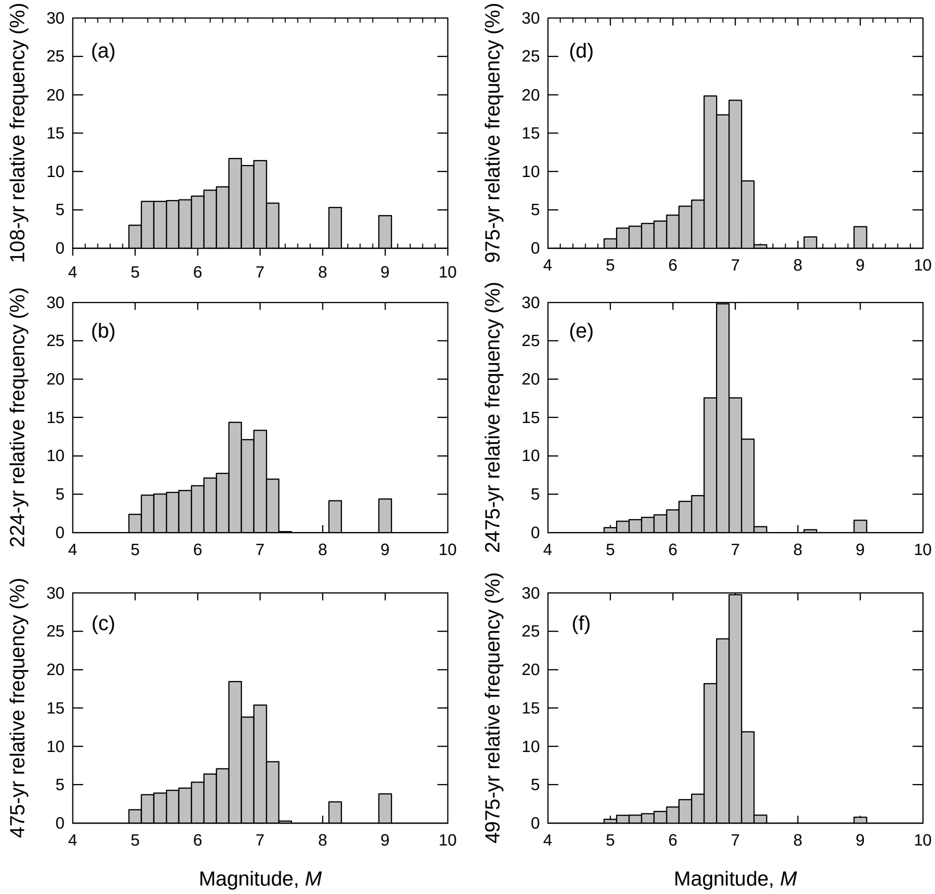

Figure 3.2. Distributions of magnitude contributing to peak rock outcrop acceleration for different return periods in Seattle, Washington (a) T_R = 108 yrs, (b) T_R = 224 yrs, (c) T_R = 475 yrs, (d) T_R = 975 yrs, (e) T_R = 2,475 yrs, and (f) T_R = 4,975 yrs.

3.2 Performance-Based Liquefaction Potential Evaluation

In practice, liquefaction potential is usually evaluated using deterministic *CRR* curves, a single ground motion hazard level, for example, for ground motions with a 475-yr return period., and a single earthquake magnitude, usually the mean or mode. In contrast, the performance-based approach incorporates probabilistic *CRR* curves and contributions from *all* hazard levels and *all* earthquake magnitudes.

The first known application of this approach to liquefaction assessment was presented by Yegian and Whitman (1978), although earthquake loading was described as a combination of earthquake magnitude and source-to-site distance rather than peak acceleration and magnitude. Atkinson et al. (1984) developed a procedure for estimation of the annual probability of liquefaction using linearized approximations of the *CRR* curves of Seed and Idriss (1983) in a deterministic manner. Marrone et al. (2003) described liquefaction assessment methods that incorporate probabilistic *CRR* curves and the full range of magnitudes and peak accelerations in a manner similar to the PBEE framework described herein. Hwang et al. (2005) described a Monte Carlo simulation-based approach that produces similar results.

PBEE is generally formulated in a probabilistic framework to evaluate the risk associated with earthquake shaking at a particular site. The risk can be expressed in terms of economic loss, fatalities, or other measures. The Pacific Earthquake Engineering Research Center (PEER) has developed a probabilistic framework for PBEE (Cornell and Krawinkler, 2000; Krawinkler, 2002; Deierlein et al., 2003) that computes risk as a function of ground shaking through the use of several intermediate variables. The ground motion is characterized by an *Intensity Measure*, *IM*, which could be any one of a number of ground motion parameters (e.g. a_{max}, Arias intensity, etc.). The effects of the *IM* on a system of interest are expressed in terms used primarily by engineers in the form of *Engineering Demand Parameters*, or *EDP*s (e.g. excess pore pressure, FS_L, etc.). The physical effects associated with the *EDP*s (e.g. settlement, lateral displacement, etc.) are expressed in terms of *Damage Measures*, or *DM*s. Finally, the risk associated with the *DM* is expressed in a form that is useful to decision-makers by means of *Decision Variables*, *DV* (e.g. repair cost, downtime, etc.). The mean annual rate of exceedance of various *DV* levels, λ_{DV}, can be expressed in terms of the other variables as

$$\lambda_{dv} = \sum_{k=1}^{N_{DM}} \sum_{j=1}^{N_{EDP}} \sum_{i=1}^{N_{IM}} P[DV > dv \mid DM = dm_k] P[DM = dm_k \mid EDP = edp_j] P[EDP = edp_j \mid IM = im_i] \Delta\lambda_{im_i} \qquad (3.1)$$

where $P[a|b]$ describes the conditional probability of a given b, and N_{DM}, N_{EDP}, and N_{IM} are the number of increments of *DM*, *EDP*, and *IM*, respectively. Extending this approach to consider epistemic uncertainty in *IM*, although not pursued in this paper, is straightforward. By integrating over the entire hazard curve (approximated by the summation over $i = 1, N_{IM}$), the performance-based approach includes contributions from all return periods, not just the return periods mandated by various codes or regulations.

Chapter 4 – Performance-Based Liquefaction Potential Analysis

One of the benefits of the PEER framework described in Chapter 3 is its modularity. The framing equation (Equation 3.1) can be broken into a series of components, which allows hazard curves for EDP and/or DM to be computed. This modularity is useful for liquefaction problems in which the EDP can represent quantities of interest such as FSL or the SPT value required to resist liquefaction.

4.1 Performance-Based Factor of Safety

For a liquefiable site, the geotechnical engineer's initial contribution to this process for evaluating liquefaction hazards comes primarily in the evaluation of P[*EDP*|*IM*]. Representing the *EDP* by FS_L and combining the probabilistic evaluation of FS_L with the results of a seismic hazard analysis allows the mean annual rate of *non*-exceedance of a selected factor of safety, fs_L, to be computed as

$$\Lambda_{FS_L}(fs_L) = \sum_{i=1}^{N_{IM}} P[FS_L < fs_L \mid IM_i] \Delta \lambda_{IM_i}, \tag{4.1}$$

The value of Λ_{FS_L} should be interpreted as the mean annual rate (or inverse of the return period) at which the actual factor of safety will be less than fs_L. Note that Λ_{FS_L} increases with increasing fs_L since weaker motions producing higher factors of safety occur more frequently than stronger motions that produce lower factors of safety. The mean annual rate of factor of safety non-exceedance is used because non-exceedance of a particular factor of safety represents an undesirable condition, just as exceedance of an intensity measure does; because lower case lambda is commonly used to represent mean annual rate of exceedance, an upper case lambda is used here to represent mean annual rate of non-exceedance. Since liquefaction is expected to occur when $CRR < CSR$ (i.e. when $fs_L < 1.0$), the return period of liquefaction corresponds to the reciprocal of the mean annual rate of non-exceedance of $fs_L = 1.0$, i.e. $T_{R,L} = 1/\Lambda_{FS_L=1.0}$.

The PEER framework assumes *IM* sufficiency, i.e. that the intensity measure is a scalar that provides all of the information required to predict the *EDP*. This sufficiency, however, does not exist for cyclic stress-based liquefaction potential evaluation procedures as evidenced by the long-recognized need for a magnitude scaling factor. Therefore, FS_L depends on more than just peak acceleration as an intensity measure, and calculation of the mean annual rate of exceeding some factor of safety against liquefaction, fs_L, can be modified as

$$\Lambda_{FS_L}(fs_L) = \sum_{j=1}^{N_M} \sum_{i=1}^{N_{a_{\max}}} P[FS_L < fs_L \mid a_{\max i}, m_j] \Delta \lambda_{a_{\max i}, m_j} \tag{4.2}$$

where N_M and $N_{a_{\max}}$ are the number of magnitude and peak acceleration increments into which "hazard space" is subdivided and $\Delta \lambda_{a_{\max i}, m_j}$ is the incremental mean annual rate of exceedance for intensity measure, $a_{\max i}$, and magnitude, m_j. The values of $\lambda_{a_{\max,m}}$ can be visualized as a series of seismic hazard curves distributed with respect to magnitude according to the results of a deaggregation analysis (Figure 3.2); therefore, their summation (over magnitude) yields the total seismic hazard curve for the site (Figure 4.1). The conditional probability term in Equation (4.2) can be calculated using the probabilistic model of Cetin et al. (2004), as described in Equation (2.2), with $CSR = CSR_{eq,i} FS^*_L$ (with $CSR_{eq,i}$ computed from $a_{\max,i}$) and $M_w = m_j$, i.e.

$$P[FS_L < fs_L \mid a_{\max i}, m_j] = \Phi\left[-\frac{(N_1)_{60}(1+\theta_1 FC) - \theta_2 \ln\left(CSR_{eq,i,j}\ fs_L\right) - \theta_3 \ln m_j - \theta_4 \ln\left(\sigma'_{vo}/p_a\right) + \theta_5 FC + \theta_6}{\sigma_\varepsilon} \right] \tag{4.3}$$

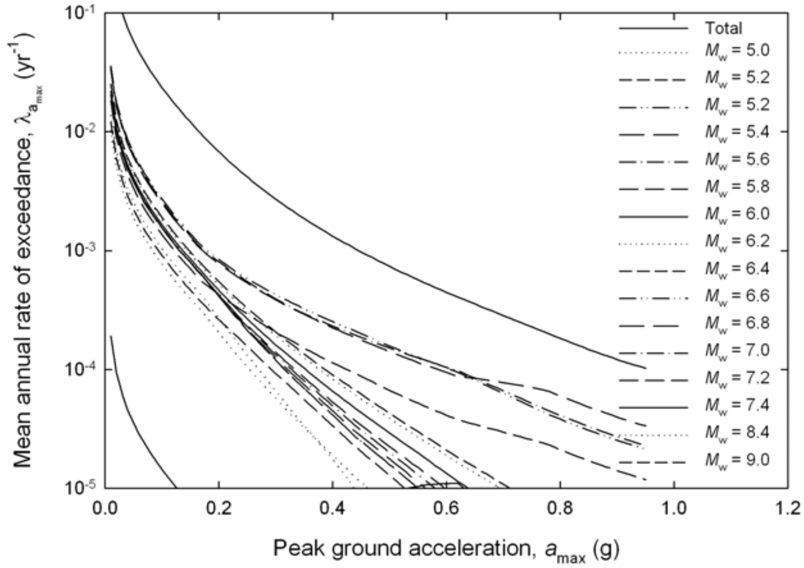

Figure 4.1. Seismic hazard curves for Seattle, Washington deaggregated on basis of magnitude. Total hazard curve is equal to sum of hazard curves for all magnitudes.

4.2 Performance-Based Required Blowcount

Another way of characterizing liquefaction potential is in terms of the liquefaction resistance required to produce a desired level of performance. For example, the SPT value required to resist liquefaction, N_{req}, can be determined at each depth of interest. The difference between the actual SPT resistance and the required SPT resistance would provide an indication of how much soil improvement might be required to bring a particular site to an acceptable factor of safety against liquefaction. Given that liquefaction would occur when $N < N_{\text{req}}$, or when $FS_{\text{L}} < 1.0$, then $P[N < N_{\text{req}}] = P[FS_{\text{L}} < 1.0]$. The PBEE approach can then be applied in such a way as to produce a mean annual rate of exceedance for N^*_{req}

$$\lambda_{N_{req}}(n_{req}) = \sum_{j=1}^{N_M} \sum_{i=1}^{N_{a_{\max}}} P[N_{req} > n_{req} \mid a_{\max i}, m_j] \Delta \lambda_{a_{\max i}, m_j} \tag{4.4}$$

where

$$P[N_{req} > n_{req} \mid a_{\max i}, m_j] = \Phi\left[-\frac{n_{req}(1+\theta_1 FC) - \theta_2 \ln CSR_{eq,i,j} - \theta_3 \ln m_j - \theta_4 \ln\left(\sigma'_{vo}/p_a\right) + \theta_5 FC + \theta_6}{\sigma_\varepsilon} \right] \tag{4.5}$$

The value of n_{req} can be interpreted as the SPT resistance required to produce the desired performance level for shaking with a return period of $1/\lambda_{N_{req}}(n_{req})$.

4.3 Comparison of Conventional and Performance-Based Approaches

Conventional procedures provide a means for evaluating the liquefaction potential of a soil deposit for a given level of loading. When applied consistently to different sites in the same seismic environment, they provide a consistent indication of the likelihood of liquefaction (expressed in terms of FS_{L} or P_{L}) at those sites. The degree to which they provide a consistent indication of liquefaction likelihood when applied to sites in *different* seismic environments, however, has not been established. That issue is addressed in the remainder of this paper.

4.3.1 Idealized Site

Potentially liquefiable sites around the world have different likelihoods of liquefaction due to differences in site conditions (which strongly affect liquefaction resistance) and local seismic environments (which strongly affect loading). The effects of seismic environment can be isolated by considering the liquefaction potential of a single soil profile placed at different locations.

Figure 4.2 shows the subsurface conditions for an idealized, hypothetical site with corrected SPT resistances that range from relatively low ($(N_1)_{60} = 10$) to moderately high ($(N_1)_{60} = 30$). Using the cyclic stress-based approach, the upper portion of the saturated sand would be expected to liquefy under moderately strong shaking. The wide range of smoothly increasing SPT resistance, while perhaps unlikely to be realized in a natural depositional environment, is useful for illustrating the main points of this paper.

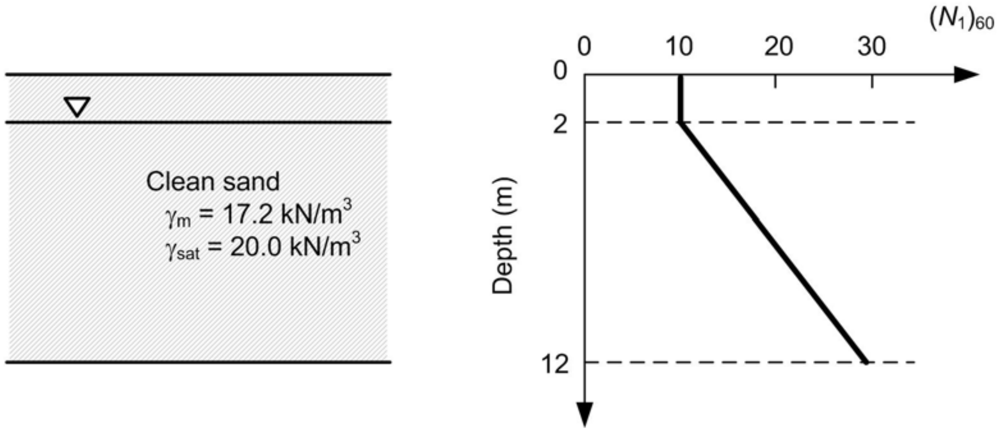

Figure 4.2. Subsurface profile for idealized site.

4.3.2 Locations

In order to illustrate the effects of different seismic environments on liquefaction potential, the hypothetical site was assumed to be located in each of the 10 U.S. cities listed in Table 4.1. For each location, the local seismicity was characterized by the probabilistic seismic hazard analyses available from the U.S. Geological Survey (using 2002 interactive deaggregation link with listed latitudes and longitudes). In addition to being spread across the United States, these locations represent a wide range of seismic environments; the total seismic hazard curves for each of the locations are shown in Figure 4.3. The seismicity levels vary widely – 475-yr peak acceleration values range from 0.12g (Butte) to 0.66g (Eureka). Two of the locations (Charleston and Memphis) are in areas of low recent seismicity with very large historical earthquakes, three (Seattle, Portland, and Eureka) are in areas subject to large-magnitude subduction earthquakes, and two (San Francisco and San Jose) are in close proximity (~ 60 km) in a very active environment.

Table 4.1. Peak ground surface (quaternary alluvium) acceleration hazard information for 10 U.S. cities.

Location	Lat. (N)	Long. (W)	475-yr a_{max}	2,475-yr a_{max}
Butte, MT	46.003	112.533	0.120	0.225
Charleston, SC	32.776	79.931	0.189	0.734
Eureka, CA	40.802	124.162	0.658	1.023
Memphis, TN	35.149	90.048	0.214	0.655
Portland, OR	45.523	122.675	0.204	0.398

Salt Lake City, UT	40.755	111.898	0.298	0.679
San Francisco, CA	37.775	122.418	0.468	0.675
San Jose, CA	37.339	121.893	0.449	0.618
Santa Monica, CA	34.015	118.492	0.432	0.710
Seattle, WA	47.530	122.300	0.332	0.620

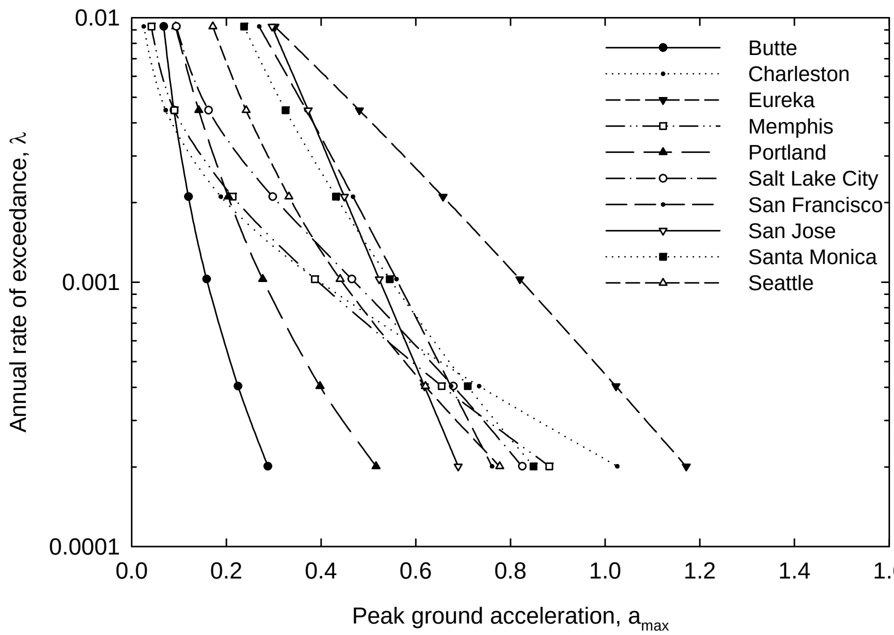

Figure 4.3. USGS total seismic hazard curves for quaternary alluvium conditions at different site locations.

4.3.3 Conventional Liquefaction Potential Analyses

Two sets of conventional deterministic analyses were performed to illustrate the different degrees of liquefaction potential of the hypothetical soil profile at the different site locations. The first set of analyses was performed using the NCEER procedure with 475-yr peak ground accelerations and magnitude scaling factors computed using the mean magnitude from the 475-yr deaggregation of peak ground acceleration. The second set of analyses was performed using Equation (2.2) with $P_L = 0.6$ to produce a deterministic approximation to the NCEER procedure; these analyses will be referred to hereafter as NCEER-C analyses (it should be noted that, although applied deterministically in this paper, the NCEER-C approximation to the NCEER procedure used here is *not* equivalent to the deterministic procedure recommended by Cetin et al. (2004)). In all analyses, the peak ground surface accelerations were computed from the peak rock outcrop accelerations obtained from the USGS 2002 interactive deaggregations using a Quaternary alluvium amplification factor (Stewart et al., 2003),

$$F_a = \frac{a_{\max,surface}}{a_{\max,rock}} = \exp\left[-0.15 - 0.13 \ln a_{\max,rock}\right] \tag{4.6}$$

The amplification factor was applied deterministically so the uncertainty in peak ground surface acceleration is controlled by the uncertainties in the attenuation relationships used in the USGS PSHAs. The uncertainties in peak ground surface accelerations for soil sites are usually equal to or somewhat lower than those for rock sites (e.g. Toro et al., 1997; Stewart et al., 2003).

The results of the first set of analyses are shown in Figure 4.4. Figure 4.4(a) shows the variation of FS_L with depth for the hypothetical soil profile at each location. The results are, as expected, consistent with the seismic hazard curves – the locations with the highest 475-yr a_{max} values have the lowest factors of safety against liquefaction. Figure 4.4(b) expresses the results of the conventional analyses in a different way – in terms of $N_{req}^{\det}$, the SPT resistance required to produce a performance level of FS_L = 1.2 with the 475-yr ground motion parameters for each location. The $(N_1)_{60}$ values for the hypothetical soil profile are also shown in Figure 4.4(b), and can be seen to exceed the $N_{req}^{\det}$ values at all locations/depths for which $FS_L > 1.2$. It should be noted that $N_{req}^{\det} \leq 30$ for all cases since the NCEER procedure implies zero liquefaction potential (infinite FS_L) for $(N_1)_{60} > 30$.

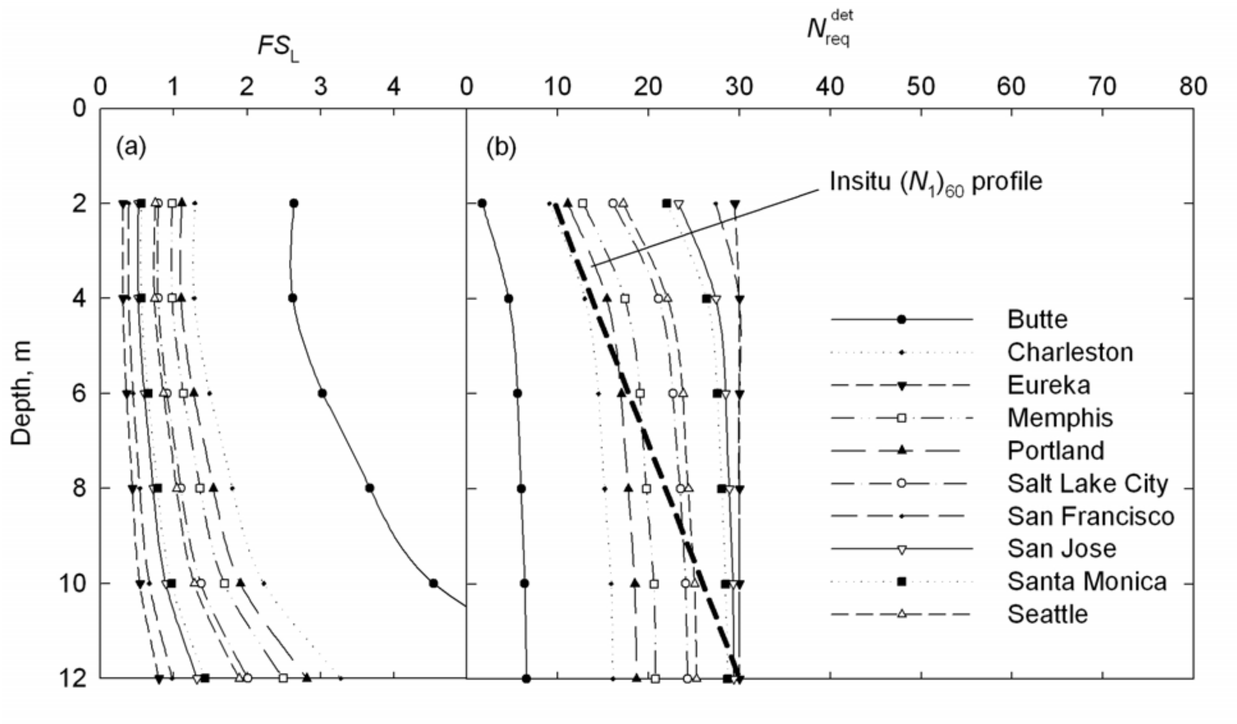

Figure 4.4. Profiles of (a) factor of safety against liquefaction and (b) required SPT resistance obtained using NCEER deterministic procedure with 475-yr ground motions.

The results of the second set of analyses are shown in Figure 4.5, both in terms of FS_L and N_{req}^{det}. The FS_L and N_{req}^{det} values are generally quite similar to those from the first set of analyses, except that required SPT resistances are slightly in excess of 30 (as allowed by the NCEER-C procedure) for the most seismically active locations in the second set. The similarity of these values confirms the approximation of the NCEER procedure by the NCEER-C procedure.

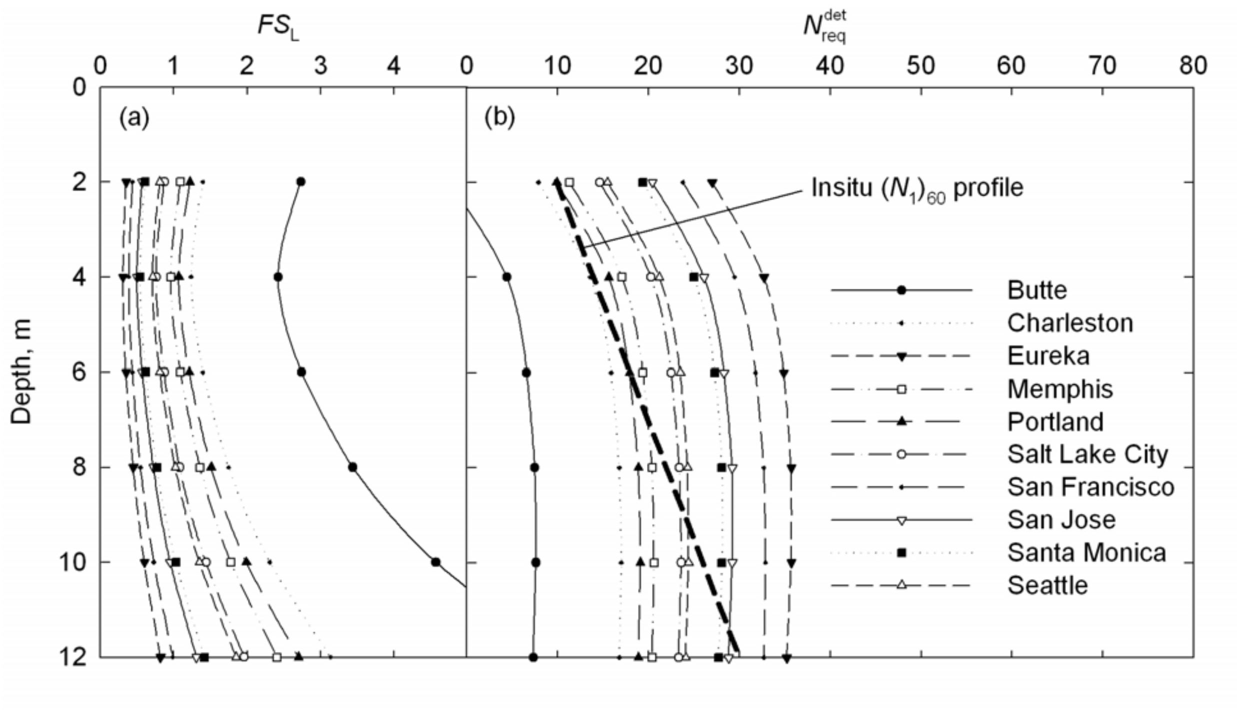

Figure 4.5. Profiles of (a) factor of safety against liquefaction and (b) required SPT resistance obtained using NCEER-C deterministic procedure for 475-yr ground motions.

4.3.4 Performance-Based Liquefaction Potential Analyses

The performance-based approach, which allows consideration of all ground motion levels and fully probabilistic computation of liquefaction hazard curves, was applied to each of the site locations. Figure 4.6 illustrates the results of the performance-based analyses for an element of soil near the center of the saturated zone (at a depth of 6 m, at which $(N_1)_{60}$ = 18 for the hypothetical soil profile). Figure 4.6(a) shows factor of safety hazard curves, and Figure 4.6(b) shows hazard curves for N_{req}^{PB}, the SPT resistance required to resist liquefaction. Note that the SPT resistances shown in Figure 4.6(b) are those at which liquefaction would actually be expected to occur, rather than the values at which FS_L would be as low as 1.2 (corresponding to a conventionally liquefaction resistant soil as defined previously), which were plotted in Figures 4.4 and 4.5. Therefore, the mean annual rates of exceedance in Figure 4.6 are equal at each site location for FS_L = 1.0 and N_{req}^{PB} = 18.

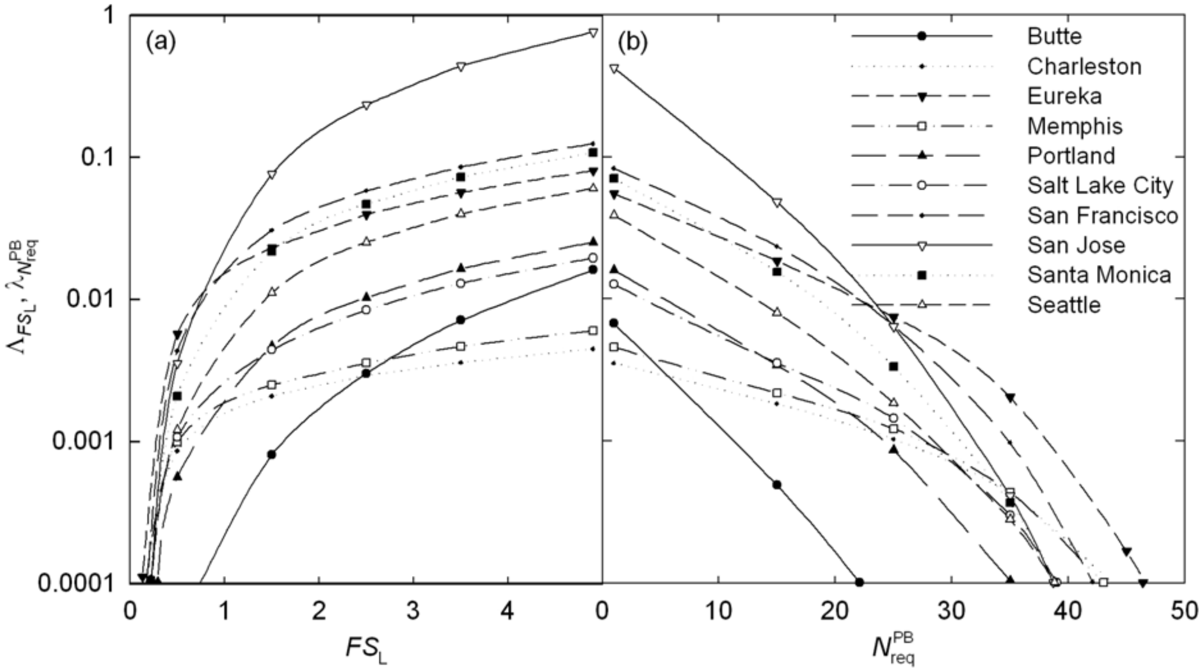

Figure 4.6. Seismic hazard curves for 6-m depth: (a) factor of safety against liquefaction, FS_L for $(N_1)_{60}$ = 18, and (b) required SPT resistance, N_{req}^{PB}, for FS_L = 1.0.

4.3.4.1 Equivalent Return Periods

The results of the conventional deterministic analyses shown in Figures 4.4 and 4.5 can be combined with the results of the performance-based analyses shown in Figure 4.6 to evaluate the return periods of liquefaction produced in different areas by consistent application of conventional procedures for evaluation of liquefaction potential. For each site location, the process is as follows:

1. At the depth of interest, determine the SPT resistance required to produce a factor of safety of 1.2 using the conventional approach (from either Figure 4.4(b) or 4.5(b)). At that SPT resistance, the soils at that depth would have an equal liquefaction potential (i.e. FS_L =1.2 with a 475-yr ground motion) at all site locations as evaluated using the conventional approach.
2. Determine the mean annual rate of exceedance for the SPT resistance from Step 1 using results of the type shown in Figure 4.6(b) for each depth of interest. Since Figure 4.6(b) shows the SPT resistance for FS_L = 1.0, this is the mean annual rate of liquefaction for soils with this SPT resistance at the depth of interest.
3. Compute the return period as the reciprocal of the mean annual rate of exceedance.
4. Repeat Steps 1-3 for each depth of interest.

This process was applied to all site locations in Table 2 to evaluate the return period for liquefaction as a function of depth for each location; the calculations were performed using 475-yr ground motions and again using 2,475-yr ground motions.

Figure 4.7 shows the results of this process for both sets of conventional analyses. It is obvious from Figure 4.7 that consistent application of the conventional procedure produces inconsistent return periods, and therefore different actual likelihoods of liquefaction, at the different site locations. Examination of the return period curves shows that they are nearly vertical at depths greater than about 4 m, indicating that the deterministic procedures are relatively unbiased with respect to SPT resistance. The greater verticality of the curves based on the NCEER-C analyses results from the consistency of the shapes of those curves and the constant P_L curves given by Equation (2.2), which were used in the performance-based analyses. Differences between the shapes of the NCEER curve (Figure 2.1a) and the curves (Figure 2.1b), particularly for sites subjected to very strong shaking (hence, very high CSRs) such as San Francisco and Eureka, contribute to depth-dependent return periods for the NCEER results.

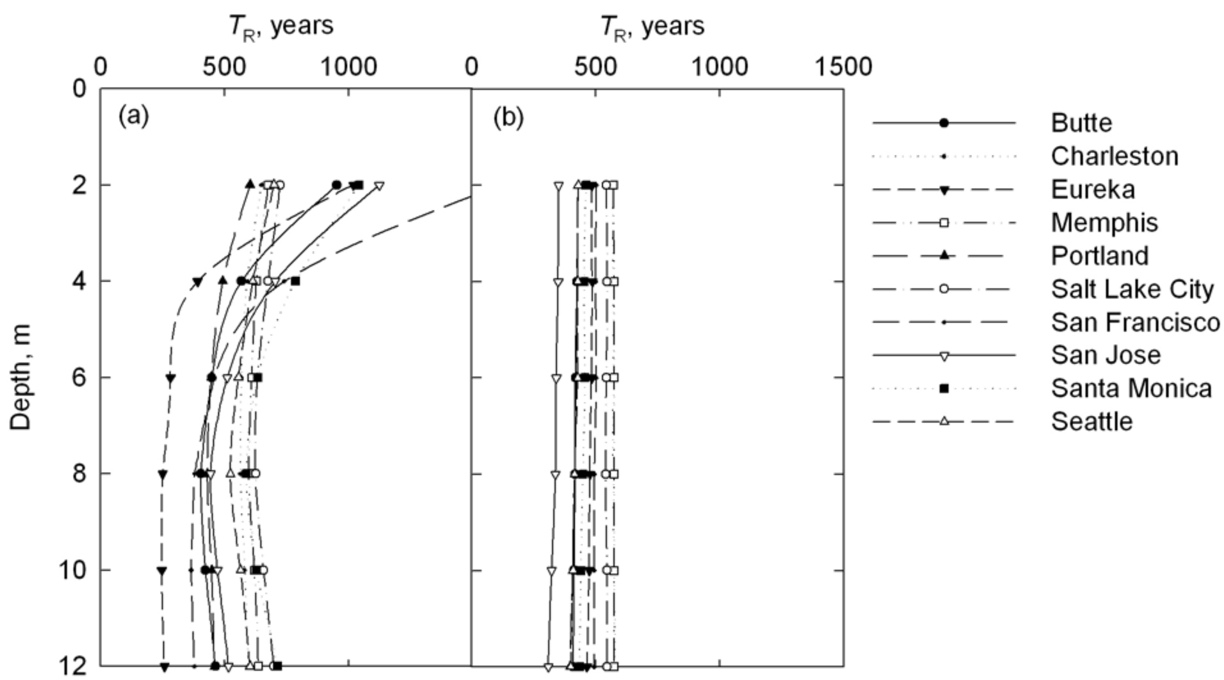

Figure 4.7. Profiles of return period of liquefaction for sites with equal liquefaction potential as evaluated by (a) NCEER procedure and (b) NCEER-C procedure using 475-yr ground motion parameters.

Table 4.2 shows the return periods of liquefaction at a depth of 6 m (the values are approximately equal to the averages over the depth of the saturated zone for each site location) for conditions that would be judged as having equal liquefaction potential using conventional procedures. Using both the NCEER and NCEER-C procedures, the actual return periods of liquefaction can be seen to vary significantly from one location to another, particularly for the case in which the conventional procedure was used with 2,475-yr motions.

Table 4.2. Liquefaction return periods for 6 m depth in idealized site at different site locations based on conventional liquefaction potential evaluation using 475-yr and 2,475-yr motions.

Location	475-yr motions		2,475-yr motions	
	NCEER	NCEER-C	NCEER	NCEER-C
Butte, MT	348	418	1592	2304
Charleston, SC	532	571	1433 [a]	2725
Eureka, CA	236 [a]	483	236 [a]	1590
Memphis, TN	565	575	1277 [a]	2532
Portland, OR	376	422	1675	1508
Salt Lake City, UT	552	543	1316 [a]	2674
San Francisco, CA	355 [a]	503	355 [a]	1736
San Jose, CA	360	341	532 [a]	1021
Santa Monica, CA	483	457	794 [a]	1901
Seattle, WA	448	427	1280 [a]	2155
[a] upper limit of $(N_1)_{60}$ = 30 implied by NCEER procedure reached.				

The actual return periods depend on the seismic hazard curves and deaggregated magnitude distributions, and are different for the NCEER and NCEER-C procedures. Using the NCEER procedure with 475-yr motions, the actual return periods of liquefaction range from as short as 236 yrs (for Eureka, which is affected by the $(N_1)_{60}$ = 30 limit implied by the NCEER procedure) to 565 yrs (Memphis); the corresponding 50-yr probability of liquefaction (under the Poisson assumption) in Eureka would be more than double that in Memphis. The return periods computed using the NCEER-C procedure with 475-yr motions are more consistent, but still range from 341 yrs (San Jose) to about 570 yrs (Charleston and Memphis).

If deterministic liquefaction potential evaluations are based on 2,475-yr ground motions using the NCEER procedure, the implied limit of $(N_1)_{60}$ = 30 produces highly inconsistent actual return periods – the 50-yr probability of liquefaction in Eureka would be more than six times that in Portland. All but two of the 10 locations would require $(N_1)_{60}$ = 30 according to that procedure and, as illustrated in Figure 9(b), the return periods for N_{req}^{PB} = 30 vary widely in the different seismic environments. The variations are smaller but still quite significant using the NCEER-C procedure.

Differences in regional seismicity can produce significant differences in ground motions at different return periods. Leyendecker et al. (2000) showed that short-period (0.2 sec) spectral acceleration, for example, increased by about 50% when going from return periods of 475 yrs to 2,475 yrs in Los Angeles and San Francisco but by 200 - 500% or more in other areas of the country. The position and slope of the peak acceleration hazard curve clearly affect the return period of liquefaction. However, the regional differences in magnitude distribution (i.e. the relative contribution to peak acceleration hazard from each magnitude) also contribute to differences in return period; San Francisco and San Jose have substantially different return periods for liquefaction despite the similarity of their hazard curves because the relative contributions of large magnitude earthquakes on the San Andreas fault are higher for San Francisco than for San Jose.

Chapter 5 – A Simplified, Mapping-Based Procedure

The calculations involved in performing a complete performance-based evaluation of liquefaction potential are not extraordinarily difficult, but they are voluminous and involve dealing with quantities that are not familiar to most practicing engineers. The calculations can be coded into a computer program for site-specific, complete performance-based analyses.

An alternative procedure would be to arrange the calculations to produce a single scalar parameter that can be used with a simple correction procedure to closely approximate the results of a complete performance-based analysis. With such an approach, one analyst could compute values of the scalar parameter for different return periods on a grid of locations and map them, much as the USGS currently maps ground motion parameters (e.g., peak acceleration, response spectral ordinates). This chapter describes the development and validation of such a procedure.

5.1 Relative Penetration Resistance

The Kramer and Mayfield (2007) procedure allowed liquefaction hazards to be expressed in two ways – in terms of a factor of safety against liquefaction (Equation 3) or in terms of a relative penetration resistance,

$$\Delta N_L = N_{site} - N_{req} \tag{5.1}$$

where N_{site} is the corrected insitu SPT resistance, $(N_1)_{60,cs}$, for the soil element of interest, and N_{req} is the corrected SPT resistance to produce FS_L for the same soil element. Figure 5.1 illustrates the relationship between FS_L and ΔN_L; it is apparent that either FS_L or ΔN_L can be used as indicators of liquefaction potential.

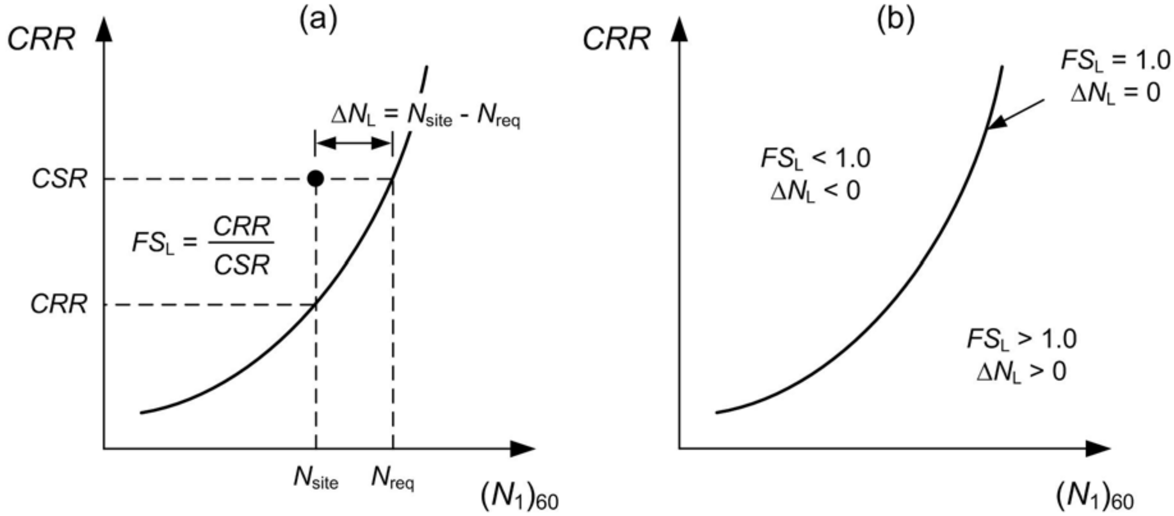

Figure 5.1. Schematic illustration of (a) definitions of FS_L and ΔN_L, and (b) relationship between FS_L and ΔN_L.

5.2 Liquefaction Hazard Curves

Chapter 4 presented the development of liquefaction hazard curves, i.e., plots showing the mean annual rate of non-exceedance of different factors of safety and the mean annual rate of exceedance of different values of N_{req}. Figure 5.2 shows a simple, idealized, reference soil profile and FS_L and N_{req} hazard curves for an element of soil at a depth of 6 m in that profile if it was located in Seattle, Washington; the assumed SPT resistance of that element is N_{site} = 18 and the seismic hazard information is from the USGS 2002 interactive deaggregation website (http://eqint.cr.usgs.gov/deaggint/2002/index.php), which provides peak acceleration data for soft rock (V_{s30} = 760 m/s) conditions and the deaggregated contributions from a range of magnitudes. The hazard curve for FS_L (Figure 5.2b) shows that the factor of safety against liquefaction would be expected to drop below 1.0 at a mean annual rate of 0.00695 yr^{-1}; hence, the return period of liquefaction for that element of soil would be 144 yrs. Figure 5.2(b) also shows that the 475-yr factor of safety (i.e., the factor of safety for λ_{FS_L} = 1/475) is 0.55. Figure 5.2(c) shows that a corrected penetration resistance of 26.2 blows/ft would be required for liquefaction of that element of soil to occur every 475 yrs (on average) in Seattle.

(a) (b) (c)

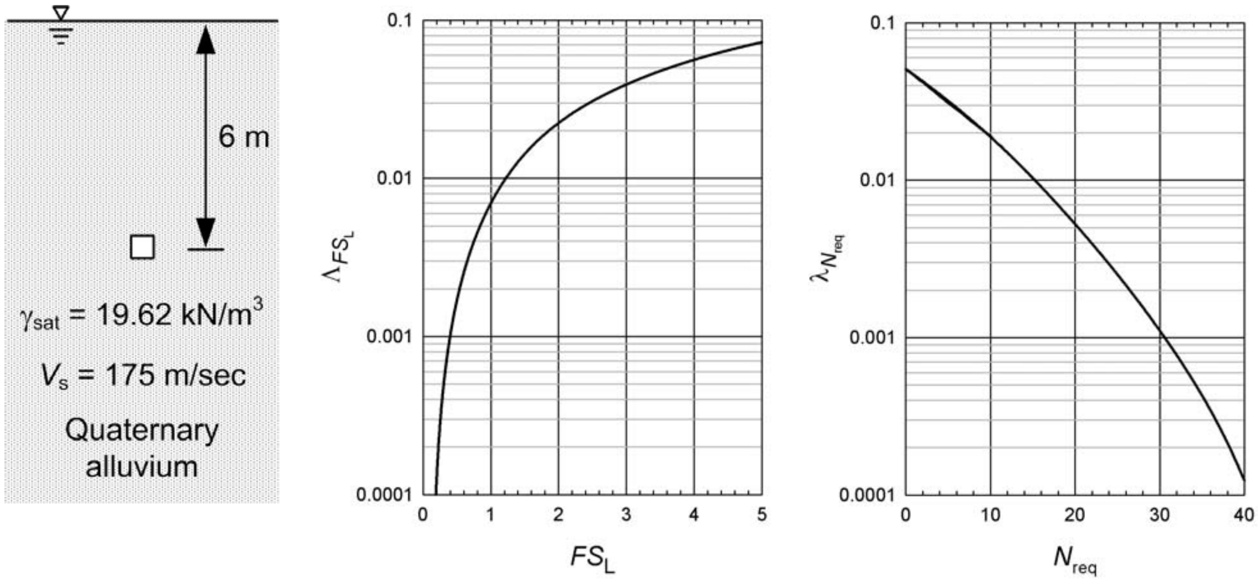

Figure 5.2. (a) Idealized reference profile with N_{site} = 18, (b) hazard curve for FS_L, (c) hazard curve for N_{req} in Seattle.

5.3 Liquefaction Hazard Maps

Liquefaction hazard curves, such as those shown in Figure 5.2, can be used to compute values of FS_L or N_{req} associated with a particular return period at a particular location Calculating the value of FS_L requires knowledge of N_{site}, but calculating the value of N_{req} does not. By assuming a reference soil profile at different locations and computing N_{req} hazard curves for each of those locations, a liquefaction hazard map can be constructed. Figure 5.3 shows contours of N_{req}^{ref} values for the 6-m-deep element in the reference profile of Figure 5.2(a) corresponding to return periods of 475 and 2,475 yrs in Washington State. Hereafter, the superscripts in N_{req}^{ref} and N_{req}^{site} will be used to distinguish between N_{req} values for the reference profile and a site-specific profile. The contours were developed from N_{req}^{ref} values computed at 247 locations on a grid spaced at 0.3 degrees latitude and 0.5 degrees longitude across the state using PSHA results obtained from the USGS 2002 interactive deaggregation website. The soft rock peak accelerations were adjusted by applying the Stewart et al. (2003) median amplification factor

$$F_a = \exp\left(a + b \ln a_{\max,rock}\right) \tag{5.1}$$

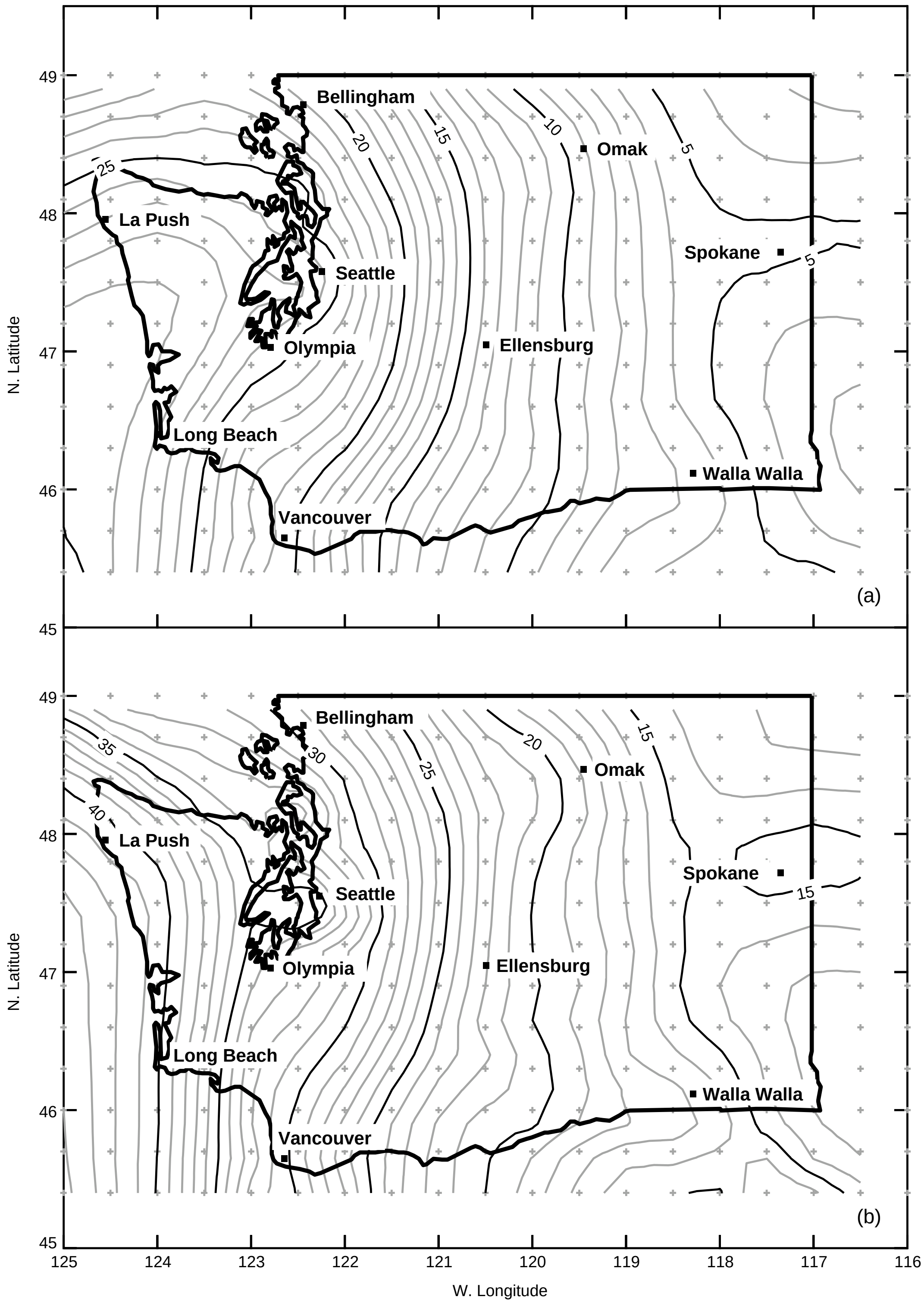

Figure 5.3. Contours of N_{req}^{ref} for Washington State: (a) 475-yr return period, and (b) 2,475-yr return period.

with the coefficients for Quaternary alluvium (a = -0.15, b = -0.13). The shapes of the N_{req}^{ref} contours generally reflect the known seismicity of Washington state, which is dominated by the Cascadia Subduction Zone in which the Juan de Fuca plate subducts beneath the curved boundary of the North American plate along coastal Washington (as well as British Columbia to the north and Oregon to the south).

5.4 Site-Specific N_{req} Adjustments

The mapped N_{req}^{ref} values shown in Figure 5.3 correspond to the particular element of soil at 6 m depth in the reference soil profile shown in Figure 12(a). In order to be broadly useful, the mapped N_{req}^{ref} values must be adjusted to provide site-specific N_{req} values for elements at depths other than 6 m in profiles with characteristics different than those of the reference profile. Recalling Equation (2.2) with coefficients from Table 2.1 with measurement/estimation errors included, and letting $(N_1)_{60,cs}^{Cetin} = (N_1)_{60}(1+0.004FC)+0.06FC$, then

$$(N_1)_{60,cs}^{Cetin} = 13.79\ln CSR_{eq} + 29.06\ln M_w + 3.82\ln\frac{\sigma'_{vo}}{p_a} - 15.25 - 4.21\Phi^{-1}(P_L) \tag{5.2}$$

Letting N_{req} = $(N_1)_{60,cs}^{Cetin}$ and using the definition of CSR_{eq}, the value of N_{req}^{ref} can be described as

$$N_{req}^{ref} = 13.79\ln\left(0.65F_a^{ref}\,a_{\max,rock}\,\frac{\sigma_{vo}^{ref}}{(\sigma'_{vo})^{ref}}\,r_d^{ref}\right) + 29.06\ln M_w + 3.82\ln\frac{(\sigma'_{vo})^{ref}}{p_a} - 15.25 - 4.21\Phi^{-1}(P_L) \tag{5.3}$$

Similarly, the value of N_{req}^{site} can be expressed as

$$N_{req}^{site} = 13.79\ln\left(0.65F_a^{site}\,a_{\max,rock}\,\frac{\sigma_{vo}^{site}}{(\sigma'_{vo})^{ref}}\,r_d^{site}\right) + 29.06\ln M_w + 3.82\ln\frac{(\sigma'_{vo})^{site}}{p_a} - 15.25 - 4.21\Phi^{-1}(P_L) \tag{5.4}$$

Note that the stress, amplification factor, and r_d terms in these equations are different, but the other terms are the same.

The site-specific adjustment can be expressed in terms of a blowcount adjustment, ΔN_{req}, defined such that

$$N_{req}^{site} = N_{req}^{ref} + \Delta N_{req} \tag{5.5}$$

Therefore, subtracting N_{req}^{ref} from both sides and substituting Equations (5.3) and (5.4), the blowcount adjustment can be written as

$$\Delta N_{req} = 13.79\ln\left(\frac{\sigma_{vo}^{site}/(\sigma'_{vo})^{site}}{\sigma_{vo}^{ref}/(\sigma'_{vo})^{ref}}\right) + 3.82\ln\frac{(\sigma'_{vo})^{site}}{(\sigma'_{vo})^{ref}} + 13.79\ln\frac{F_a^{site}}{F_a^{ref}} + 13.79\ln\frac{r_d^{site}}{r_d^{ref}} \qquad (5.6)$$

The terms in the blowcount adjustment can be grouped into components associated with vertical stresses, amplification behavior, and depth reduction factor behavior, giving

$$\Delta N_{req} = \Delta N_{\sigma} + \Delta N_F + \Delta N_{r_d} \qquad (5.7)$$

where

$$\Delta N_{\sigma} = 13.79\ln\left(\frac{\sigma_{vo}^{site}/(\sigma'_{vo})^{site}}{\sigma_{vo}^{ref}/(\sigma'_{vo})^{ref}}\right) + 3.82\ln\frac{(\sigma'_{vo})^{site}}{(\sigma'_{vo})^{ref}}$$

$$\Delta N_F = 13.79\ln\frac{F_a^{site}}{F_a^{ref}}$$

$$\Delta N_{r_d} = 13.79\ln\frac{r_d^{site}}{r_d^{ref}}$$

This formulation, therefore, allows a user to obtain N_{req}^{ref} at a site of interest from a map such as that shown in Figure 5.3, and then to determine N_{req}^{site} using a blowcount adjustment procedure. Two adjustment procedures, which require different levels of effort to implement, are described in the following sections.

5.4.1 Adjustment Procedure A

Substituting the reference site conditions into the individual components of the blowcount adjustment, the stress and amplification components can be expressed as

$$\Delta N_{\sigma} = 13.79\ln\left(\frac{\sigma_{vo}^{site}/(\sigma'_{vo})^{site}}{2}\right) + 3.82\ln\frac{(\sigma'_{vo})^{site}}{58.86} \qquad (5.8)$$

$$\Delta N_F = 13.79\ln\frac{F_a^{site}}{F_a^{ref}} = 13.79\left[a^{site} + 0.15 + \left(b^{site} + 0.13\right)\ln a_{\max,rock}\right] \qquad (5.9)$$

where $\left(\sigma'_{vo}\right)^{site}$ is in kPa.

Cetin et al. (2004) considered the variation of cyclic shear stress with depth to be influenced by peak acceleration, earthquake magnitude, and average shear wave velocity within the upper 12 m of a soil profile. They expressed the median value of their depth reduction factor model as

$$r_d^{site} = \frac{1 + \dfrac{-23.013 - 2.949a_{\max} + 0.999M_w + 0.0525\overline{V}_{s,12}}{16.258 + 0.201\exp(0.341(-z + 0.0785\overline{V}_{s,12} + 7.586))}}{1 + \dfrac{-23.013 - 2.949a_{\max} + 0.999M_w + 0.0525\overline{V}_{s,12}}{16.258 + 0.201\exp(0.341(0.0785\overline{V}_{s,12} + 7.586))}} \tag{5.10}$$

where $\overline{V}_{s,12}$ is the average shear wave velocity over the upper 12 m of the profile. This expression includes the variables $a_{\max}$ and M_w, which are used in the N_{req}^{ref} integration (Equation 7). Parametric studies indicate that r_d is relatively insensitive to combinations of $a_{\max}$ and M_w that typically affect liquefaction hazards; an observation at least partly explained by the fact that both variables affect the numerator and denominator of the r_d expression similarly. Figure 5.4 shows median r_d values for 20 combinations of $a_{\max}$ and M_w that represent the 475- and 2,475-yr peak accelerations and mean (deaggregated) magnitudes for 10 cities across the United States. Even with $a_{\max}$ values ranging from 0.12 g to 1.02 g and mean M_w values ranging from 5.97 to 7.70, the median r_d values fall within a relatively narrow range. Substituting $a_{\max}$ = 0.39g and M_w = 6.5 into Equation 17 produces r_d^{site} values that match the mean curve shown in Figure 5.4 very closely (maximum error of 0.08%). Due to this lack of sensitivity, it is reasonable to compute r_d^{site} for Adjustment Procedure A using the ground surface $a_{\max}$ value and mean M_w value corresponding to the return period of interest instead of computing it for each combination of $a_{\max}$ and M_w in the N_{req} integration.

$$\Delta N_{r_d} = 13.79\ln\frac{r_d^{site}}{0.889} \tag{5.11}$$

With Equations 5.8, 5.9, and 5.11, computing the blowcount adjustments involves computing the site-specific total and effective vertical stresses at each depth of interest, determining the appropriate site amplification coefficients within the framework of the Stewart et al. (2003) expression (Equation 5.1), and computing the Cetin et al. value of r_d at each depth of interest.

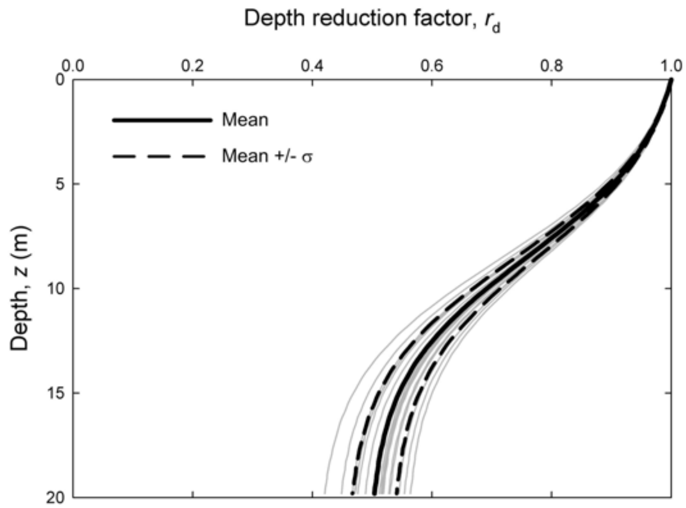

Figure 5.4. Computed median r_d profiles with $V_{s,12}$ = 175 m/s for 475-yr and 2,475-yr peak acceleration and mean magnitude for Butte, MT; Charleston, SC, Eureka, CA; Memphis, TN; Portland, OR; Salt Lake City, UT; San Francisco, CA; San Jose, CA; Santa Monica, CA; and Seattle, WA.

5.4.2 Adjustment Procedure B

Since both stresses and r_d vary significantly with depth, the development of a simpler alternative adjustment procedure was investigated. The intent of this alternative was to produce simplified depth-related expressions for ΔN_σ and ΔN_{r_d} that could be expressed in chart form for rapid estimation of ΔN_σ and ΔN_{r_d}. The ΔN_F adjustment for Procedure B is the same as for Procedure A and is not repeated in the following discussion.

5.4.2.1 Stress Component

The densities of most inorganic soils fall within a relatively narrow range, at least compared to many other soil properties. For a site with a uniform density profile and a ground water table at depth, $z = z_w$, the initial total and effective vertical stresses are given by

$$\sigma_{vo}^{site} = \gamma_d z_w + \gamma_{sat} (z - z_w) \tag{5.12a}$$

$$(\sigma'_{vo})^{site} = \gamma_d z_w + \gamma_b (z - z_w) \tag{5.12b}$$

where the dry unit weight, γ_d, saturated unit weight, γ_{sat}, and buoyant unit weight, γ_b, are functions of soil void ratio (and specific gravity of solids and unit weight of water, which are assumed to be constants). The ratio of total to effective vertical stress at some depth, $z \geq z_w$, can therefore be written as

$$\frac{\sigma_{vo}^{site}}{(\sigma'_{vo})^{site}} = \frac{G_s + e^{site}(1 - z_w / z)}{G_s - 1 + z_w / z} \tag{5.13}$$

For the reference site, G_s^{ref} = 2.67, e^{ref} = 0.67, z_w = 0, and $\sigma_{vo}^{ref} / (\sigma'_{vo})^{ref}$ = 2, so

$$\frac{\sigma_{vo}^{site} / (\sigma'_{vo})^{site}}{\sigma_{vo}^{ref} / (\sigma'_{vo})^{ref}} = \frac{G_s + e^{site}(1 - z_w / z)}{2(G_s - 1 + z_w / z)} \tag{5.14}$$

and

$$\frac{(\sigma'_{vo})^{site}}{(\sigma'_{vo})^{ref}} = \frac{z(G_s - 1 + z_w / z)}{6(1 + e^{site})} \tag{5.15}$$

Therefore

$$\Delta N_\sigma = 13.79 \ln\left[\frac{G_s + e^{site}(1 - z_w / z)}{2(G_s - 1 + z_w / z)}\right] + 3.82 \ln\left[\frac{z(G_s - 1 + z_w / z)}{6(1 + e^{site})}\right] \tag{5.16}$$

Assuming that G_s and e^{site} are the same as in the reference profile, the expression for ΔN_σ depends solely on z and z_w, i.e.,

$$\Delta N_\sigma = 13.79 \ln\left[\frac{1 - 0.2 z_w / z}{1 + 0.6 z_w / z}\right] + 3.82 \ln\left[\frac{z}{6}(1 + 0.6 z_w / z)\right] \tag{5.17}$$

Figure 5.5 illustrates the variation of ΔN_σ with depth for different groundwater table depths using Equation (5.17). The sensitivity of Equation (5.16) to e^{site} is quite low – an e^{site} value of 0.8 (very loose for most naturally deposited sands) would increase ΔN_σ by only 0.23 blows/ft, and an e^{site} value of 0.5 (quite dense for most potentially liquefiable sands) would decrease ΔN_σ by 0.29 blows/ft; this insensitivity suggests that the assumption of $e^{site} = e^{ref}$ should not significantly affect the accuracy of ΔN_σ.

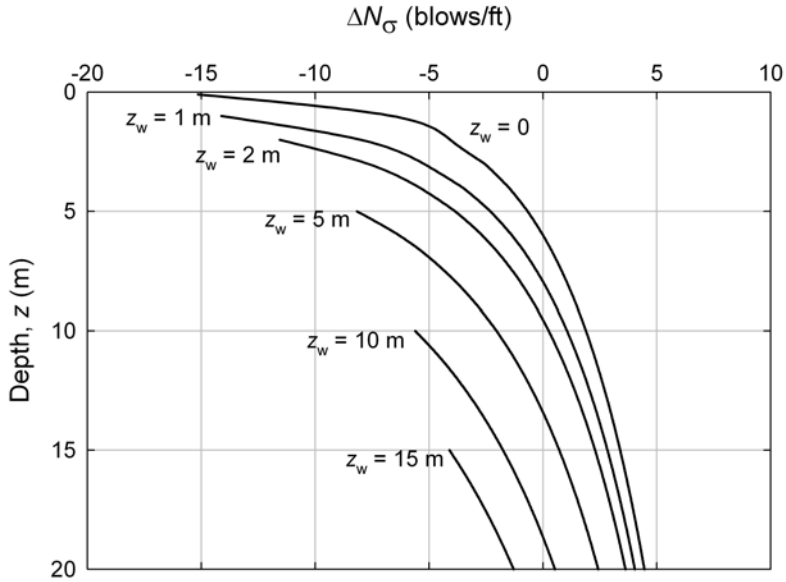

Figure 5.5. Stress-related component of Adjustment Procedure B.

5.4.2.2 Depth Reduction Factor Component

Figure 14 showed the relative insensitivity of r_d to a_{max} and M_w. Using a combination of a_{max} and M_w that correspond to the mean curve in Figure 5.4, and recognizing that the reference profile has $\overline{V}_{s,12}^{ref}$ =175 m/s, z^{ref} = 6 m, and r_d^{ref} =0.866, the depth reduction factor adjustment component can be written as a function of only depth and mean shear wave velocity,

$$\Delta N_{r_d} = 13.792\left[\ln\left(\frac{\dfrac{-1.353+0.0525\overline{V}_{s,12}+2.671\exp(0.0268\overline{V}_{s,12}-0.341z)}{-1.353+0.0525\overline{V}_{s,12}+2.671\exp(0.0268\overline{V}_{s,12})}}{\dfrac{16.258+2.671\exp(0.0268\overline{V}_{s,12}-0.341z)}{16.258+2.671\exp(0.0268\overline{V}_{s,12})}}\right)+0.118\right] \quad (5.18)$$

Figure 5.6 shows the variation of ΔN_{r_d} with depth and shear wave velocity; this component of the correction can be seen to be quite sensitive to both depth and mean shear wave velocity.

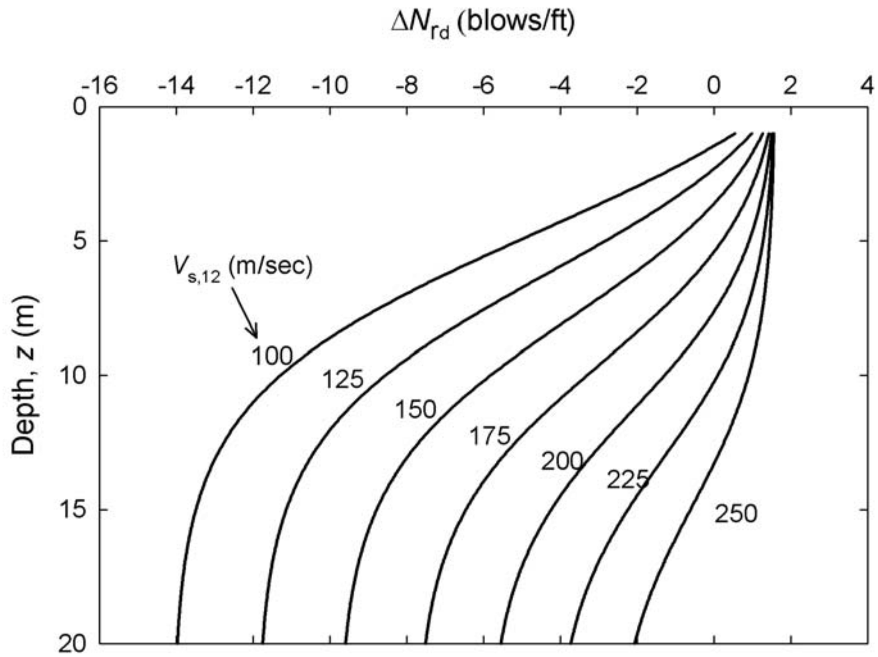

Figure 5.6. Depth reduction factor-related component of Adjustment Procedure B.

5.5 Relationship between ΔN_L and FS_L

Using mapped values of N_{req}^{ref} and either of the previously discussed adjustment procedures, site-specific estimates of $\Delta N_L = N_{site} - N_{req}^{site}$ can be obtained for a particular element of soil. While ΔN_L was shown previously to provide the same basic information, most engineers are accustomed to expressing liquefaction potential in terms of a factor of safety. Therefore, it would be useful to relate ΔN_L to FS_L. The site-specific factor of safety can be written as

$$FS_L^{site} = \frac{CRR}{CSR} = \frac{CRR(N_{site})}{CRR(N_{req}^{site})} \tag{5.19}$$

The Cetin et al. (2004) model can be rearranged to express *CRR* as

$$CRR = \exp\left[\frac{N_{req}^{Cetin} - 29.06\ln M_w - 3.82\ln\left(\frac{\sigma'_{vo}}{p_a}\right) + 15.25 + \sigma_\varepsilon \Phi^{-1}(P_L)}{13.79}\right] \tag{5.20}$$

Substituting Equation (27) and the appropriate values of penetration resistance into Equation (26) gives

$$FS_L^{site} = \frac{\exp\left[\dfrac{N_{site} - 29.06\ln M_w - 3.82\ln\left(\dfrac{\sigma'_{vo}}{p_a}\right) + 15.25 + \sigma_\varepsilon \Phi^{-1}(P_L)}{13.79}\right]}{\exp\left[\dfrac{N_{req}^{site} - 29.06\ln M_w - 3.82\ln\left(\dfrac{\sigma'_{vo}}{p_a}\right) + 15.25 + \sigma_\varepsilon \Phi^{-1}(P_L)}{13.79}\right]}$$

$$= \exp\left[\frac{N_{site} - N_{req}^{site}}{13.79}\right]$$

$$= 1.075^{\Delta N_L} \qquad (5.21)$$

The exponential nature of the Cetin et al. (2004) *CRR* relationship, therefore, provides a conveniently simple relationship between FS_L^{site} and ΔN_L.

5.6 Verification of Site-Specific Adjustment Procedures

The site-specific adjustments yield N_{req} values that can differ from those that would be obtained from a complete, site-specific, performance-based liquefaction potential evaluation. In the complete analysis, uncertainties in source parameters (e.g., earthquake magnitude) and ground motion parameter (e.g., peak acceleration) are combined with a probabilistic liquefaction potential analysis to yield N_{req} values with a rigorously characterized mean annual rate of exceedance (or return period). The proposed adjustment procedures, however, are applied deterministically, i.e., they are based on median relationships without explicit consideration of the dispersion about the median. The proposed Adjustment Procedure B also makes assumptions about the variations of stresses and r_d with depth that may be different than those in a site-specific analysis.

The following sections compare the results of liquefaction potential evaluations performed using the full site-specific, performance-based procedure with those obtained from mapped reference profile N_{req} values processed by both of the proposed adjustment procedures.

5.6.1 Soil Profile

Figure 5.7 shows an actual site along the Seattle waterfront. The profile consists of 1.5 m of medium dense, sandy silt underlain by about 9 m of generally loose, silty, fine to coarse sand (5-10% non-plastic fines) placed by hydraulic filling. This material is underlain by about 3.6 m of natural sandy silt (80% non-plastic fines), which lies on top of a thick sequence of very dense, glacially overconsolidated, silty, gravelly sands. The groundwater level is at about 2.4 m and the silts at the site are generally nonplastic. The computed value of $V_{s,12}$ from the shear wave velocity profile in Figure 5.7 is 137 m/s.

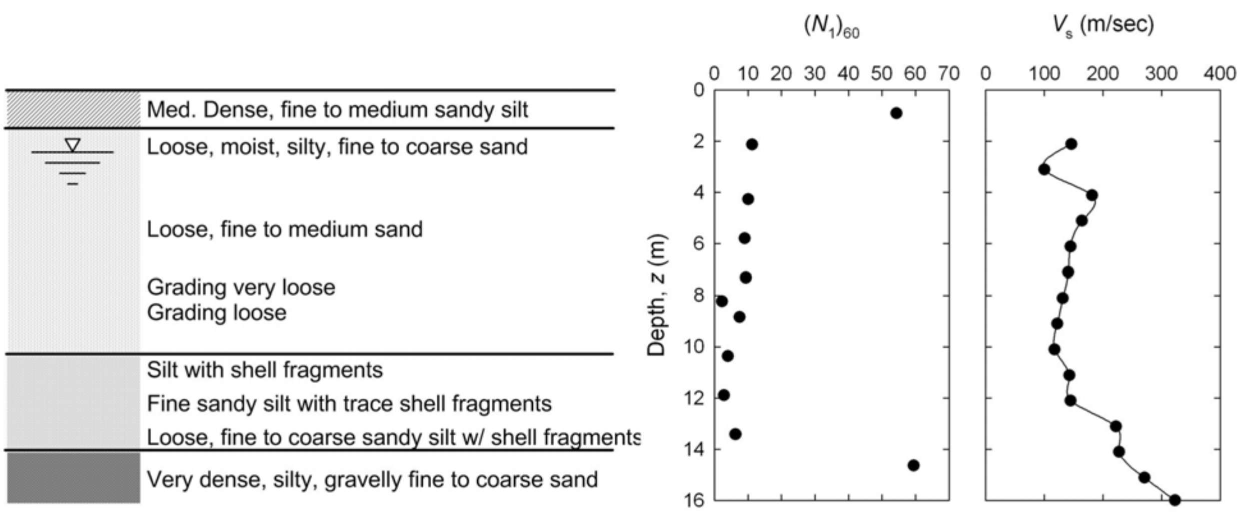

Figure 5.7. Soil profile from Seattle waterfront.

5.6.2 Site-Specific Liquefaction Potential

Figure 5.8 shows FS_L^{site} and N_{req}^{site} hazard curves for elements of soil at depths of 4.3 m (N_{site} = 10.9 blows/ft) and 8.2 m (N_{site} = 2.7 blows/ft). These hazard curves were computed using the procedure of Kramer and Mayfield (2007) and are therefore fully site-specific, i.e. they were computed for each depth considering the specific properties of the site. The hazard curves indicate 475-yr factors of safety of 0.53 and 0.28 for the shallower and deeper elements, respectively; the return periods of liquefaction for the respective elements are 135 and 46 yrs. The 475-yr N_{req}^{site} values are 19.5 and 20.0 blows/ft. Table 5. presents similar data for elements at the depths of each of the SPT tests in the saturated soils above the very dense glacial soils.

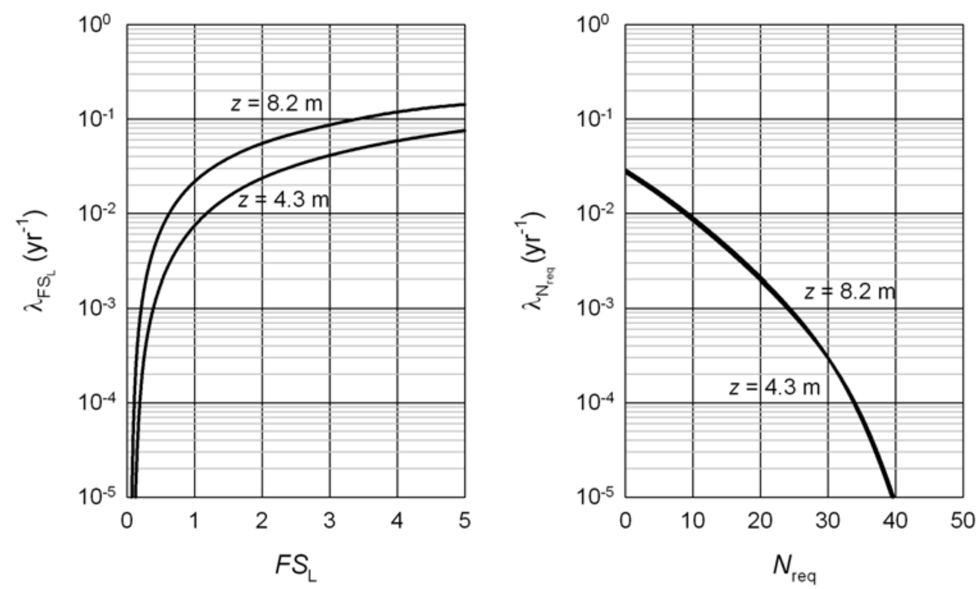

Figure 5.8. Hazard curves for FS_L and N_{req} for two elements of soil in Seattle waterfront profile.

Table 5.1. Directly computed site-specific liquefaction hazard parameters.

Depth (m)	N_{site}	475-yr N_{req}^{site}	475-yr FS_L^{site}	$T_{R,liq}$
4.3	10.9	19.5	0.54	135
5.8	9.7	20.3	0.46	104
7.3	10.1	20.2	0.48	110
8.2	2.7	20.0	0.28	46
8.8	8.2	19.9	0.43	90
10.4	7.1	19.5	0.41	82
11.9	5.5	19.3	0.37	69
13.4	10.1	19.3	0.51	124

The 475-yr N_{req}^{site} values can be seen to vary mildly with depth from values of 19.3 at the bottom of the profile to 20.3 at 5.8 m. The 475-yr FS_L^{site} values reflect the insitu SPT resistances and, therefore, fluctuate with depth from a high of 0.54 to a low of 0.28 depending on the insitu penetration resistances. Return periods of liquefaction for this profile range from 46 to 135 yrs. These relatively short return periods are consistent with the observation of instances of localized liquefaction in this general area in the 1949 Olympia, 1965 Seattle-Tacoma, and 2001 Nisqually earthquakes.

The N_{req}^{site} values obtained using both adjustment procedures are shown in Table 5.2. The N_{req}^{site} values obtained from the two adjustment procedures are in generally good agreement with those obtained from the direct, site-specific analysis (Figure 5.9a). The values from Adjustment Procedure A are in excellent agreement at shallow depths, but underpredict the directly obtained values by 0.9 blow/ft at the bottom of the profile. The values from Adjustment Procedure B underpredict the directly obtained values by amounts ranging from about 0.5 blow/ft at shallow depths to 1.3 blows/ft at the bottom of the profile.

Table 5.2. Site-specific required SPT resistances by adjustments to 475-yr Seattle N_{req}^{ref} value of 26.2.

Depth (m)	N_{site}	Procedure A				Procedure B			
		ΔN_{σ}	ΔN_{r_d}	ΔN_{req}	$N_{req}^{site,A}$	ΔN_{σ}	ΔN_{r_d}	ΔN_{req}	$N_{req}^{site,B}$
4.3	10.9	-5.82	-0.63	-6.45	19.8	-5.86	-1.20	-7.06	19.1
5.8	9.7	-3.65	-2.17	-5.83	20.4	-3.54	-2.82	-6.36	19.8
7.3	10.1	-2.15	-3.90	-6.04	20.2	-1.97	-4.60	-6.57	19.6
8.2	2.7	-1.44	-4.93	-6.37	19.8	-1.23	-5.66	-6.89	19.3
8.8	8.2	-1.02	-5.59	-6.61	19.6	-0.79	-6.33	-7.12	19.1
10.4	7.1	-0.12	-7.08	-7.20	19.0	0.14	-7.82	-7.68	18.5
11.9	5.5	0.62	-8.25	-7.62	18.6	0.90	-8.98	-8.07	18.1
13.4	10.1	1.26	-9.08	-7.82	18.4	1.55	-9.80	-8.24	18.0

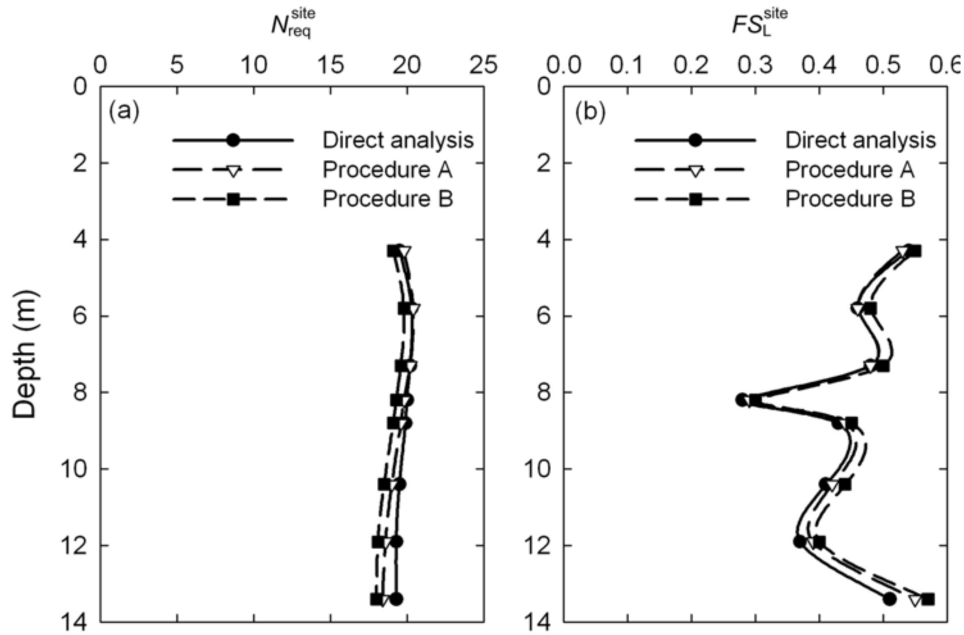

Figure 5.9. Comparison of results of direct PBEE analysis and results obtained from mapped N_{req} values: (a) 475-yr N_{req}^{site}, and (b) 475-yr FS_L^{site}.

Table 5.3 presents 475-yr FS_L values obtained using the adjusted values and the relationship between FS_L and ΔN_L given in Equation 5.21. Following from the agreement in N_{req}^{site} values, the 475-yr factor of safety values inferred from the ΔN_L values using Adjustment Procedure A are in excellent agreement (Figure 5.9b) with those obtained from the direct, site-specific analysis, particularly at shallower depths.

Table 5.3. Site-specific factor of safety values inferred from reference profile required SPT resistance.

Depth (m)	N_{site}	475-yr FS_L^{site}	Procedure A			Procedure B		
			$N_{req}^{site,A}$	$\Delta N_L^{site,A}$	$FS_L^{site,A}$	$N_{req}^{site,B}$	$\Delta N_L^{site,B}$	$FS_L^{site,B}$
4.3	10.9	0.54	19.8	-8.9	0.53	19.1	-8.3	0.55
5.8	9.7	0.46	20.4	-10.7	0.46	19.8	-10.2	0.48
7.3	10.1	0.48	20.2	-10.1	0.48	19.6	-9.6	0.50
8.2	2.7	0.28	19.8	-17.2	0.29	19.3	-16.6	0.30
8.8	8.2	0.43	19.6	-11.4	0.44	19.1	-10.9	0.45
10.4	7.1	0.41	19.0	-11.9	0.42	18.5	-11.4	0.44
11.9	5.5	0.37	18.6	-13.1	0.39	18.1	-12.6	0.40
13.4	10.1	0.51	18.4	-8.3	0.55	18.0	-7.9	0.57

The soil profile shown in Figure 5.7 was then assumed to be located in the same 10 cities used to illustrate performance-based initiation procedures by Kramer and Mayfield (2007). Table 5.4 shows the mapped N_{req}^{ref} values for each of these sites and the a_{max} and mean M_w values required for Adjustment Procedure A. These cities span a wide range of seismic activity and contain different tectonic settings. Applying the adjustment procedures to the mapped N_{req}^{ref} values for both 475- and 2,475-yr return periods and comparing with the directly computed N_{req}^{site} values at all eight depths yields the results shown in Figure 5.10. The adjusted N_{req}^{site} values are generally very close to the directly computed values – Adjustment Procedure A has a slight bias toward overprediction with a standard deviation of the differences of 0.68; Adjustment Procedure B has a slightly higher bias toward underprediction with a standard deviation of 0.62 blows/ft. The overprediction by Adjustment Procedure A is dominated by results from two cities (Charleston and Memphis, which produce the groups of points at N_{req} = 6-9 and 11-14, respectively) at the 475-yr hazard level; the highly skewed nature of the deaggregated magnitude distributions for these two cities, whose seismicity is dominated by large, historical earthquakes, gives rise to unusual combinations of a_{max} and mean magnitude (see Table 5) that produce high r_d values that are responsible for the larger difference between the computed and adjusted N_{req} values. Figure 5.11 shows comparisons of the directly computed FS_L^{site} values with the values inferred from the adjusted N_{req}^{site} values and Equation 5.21. As can be seen, the inferred values match the directly computed values very well; the Charleston and Memphis points are responsible for the most underpredicted FS_L^{site} values at the 475-yr level. Here, Adjustment Procedures A and B have slight biases toward underprediction and overprediction, respectively – the respective standard deviations of the FS_L^{site} differences for Adjustment Procedures A and B are 0.03 and 0.02.

Table 5.4. Mapped N_{req}^{ref} and ground response parameters for 10 U.S. cities.

Location	Lat.	Long.	475-yr			2,475-yr		
			N_{req}^{ref}	$a_{\max}$	M_w	N_{req}^{ref}	$a_{\max}$	M_w
Butte, MT	46.003	112.533	9.7	0.120	5.97	18.2	0.225	6.05
Charleston, SC	32.776	79.931	14.8	0.189	6.61	35.6	0.734	7.00
Eureka, CA	40.802	124.162	37.0	0.658	7.06	43.7	1.023	7.02
Memphis, TN	35.149	90.048	18.4	0.214	7.01	37.6	0.655	7.26
Portland, OR	45.523	122.675	21.4	0.204	6.81	31.5	0.398	6.73
Salt Lake City, UT	40.755	111.898	23.5	0.298	6.69	35.5	0.679	6.76
San Francisco, CA	37.775	122.418	33.5	0.468	7.43	39.7	0.675	7.50
San Jose, CA	37.339	121.893	31.3	0.449	6.73	36.5	0.618	6.65
Santa Monica, CA	34.015	118.492	29.5	0.432	6.62	36.3	0.710	6.55
Seattle, WA	47.530	122.300	26.2	0.332	6.57	35.2	0.620	6.74

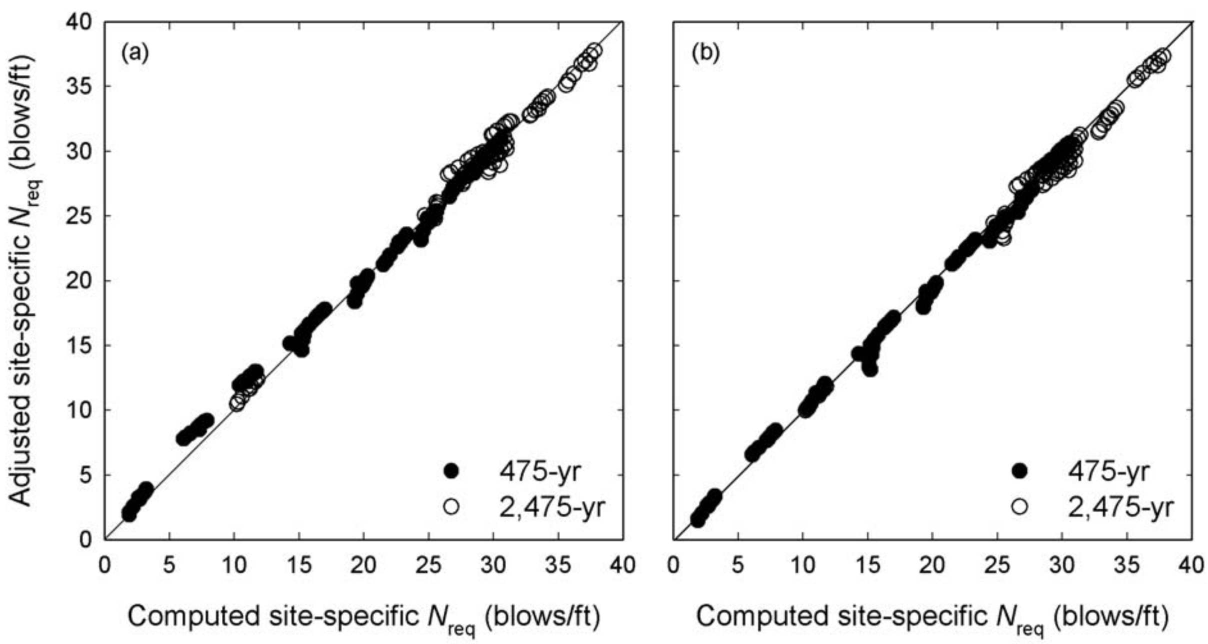

Figure 5.10. Relationship between adjusted and directly computed site-specific N_{req} values for 10 U.S. cities: (a) Adjustment Procedure A, and (b) Adjustment Procedure B.

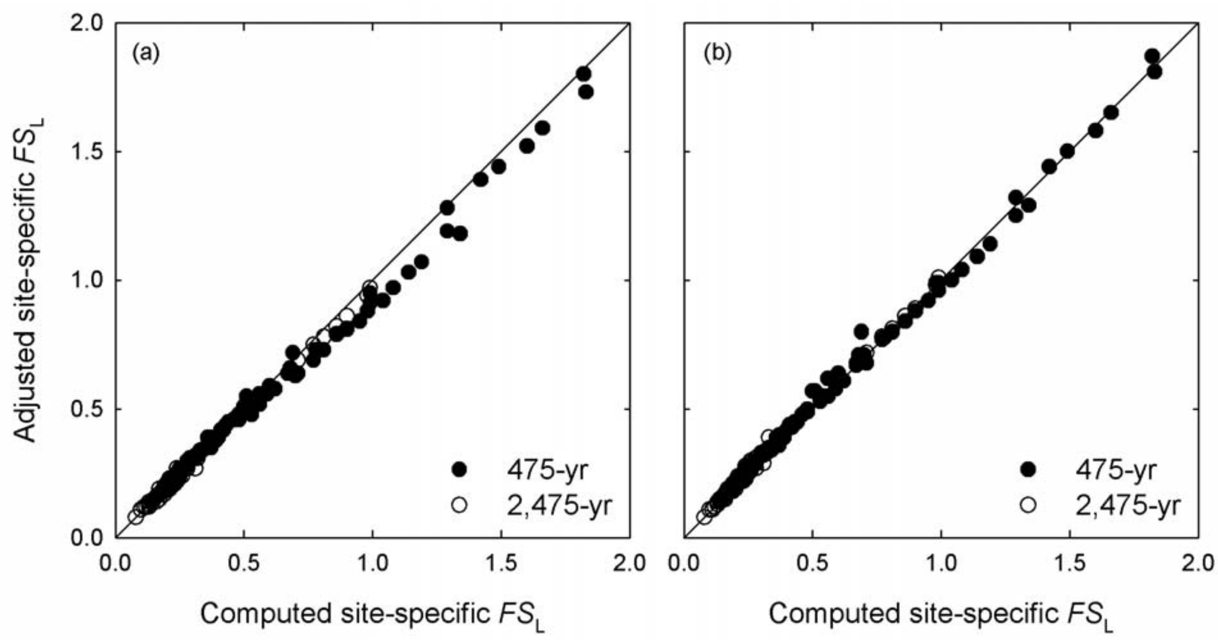

Figure 5.11. Relationship between adjusted and directly computed site-specific FS_L values for 10 U.S. cities: (a) Adjustment Procedure A, and (b) Adjustment Procedure B.

These results show that the site-specific adjustments, in combination with the mapped N_{req}^{ref} values, produce results that are very close to those obtained by performing complete performance-based liquefaction potential evaluations. Adjustment Procedure A shows slightly better (lower and more conservative bias) agreement with the results of complete performance-based evaluations, but the difference appears to be negligible for practical purposes. They also show that the site-specific N_{req} values can be used with insitu SPT resistances to compute factors of safety. The availability of mapped N_{req}^{ref} values would, therefore, provide a reasonable approximation of performance-based procedures for evaluation of liquefaction potential without requiring the user to perform the numerous calculations involved in those procedures.

Chapter 6 – Summary and Conclusions

The evaluation of liquefaction potential involves comparison of consistent measures of loading and resistance. In contemporary geotechnical engineering practice, such comparisons are commonly made using cyclic shear stresses expressed in terms of normalized cyclic stress and cyclic resistance ratios. The cyclic stress ratio is usually estimated using a simplified procedure in which the level of ground shaking is related to peak ground surface acceleration and earthquake magnitude. Criteria by which liquefaction resistance are judged to be adequate are usually expressed in terms of a single level of ground shaking.

For a given soil profile at a given location, liquefaction can be caused by a range of ground shaking levels – from strong ground motions that occur relatively rarely to weaker motions that occur more frequently. Performance-based procedures allow consideration of all levels of ground motion in the evaluation of liquefaction potential. By integrating a probabilistic liquefaction evaluation procedure with the results of a PSHA, this study made use of a methodology for performance-based evaluation of liquefaction potential. This report has also described a methodology by which a scalar quantity, expressed here as the penetration resistance required to prevent initiation of liquefaction in a particular element of soil within a reference soil profile, can be computed and mapped over a desired geographic region. It then describes two alternative procedures by which the mapped parameter can be adjusted for the effects of actual soil conditions to develop site-specific values of the required penetration resistance and inferred factor of safety. Finally, the accuracies of the site-specific adjustment procedures are demonstrated by applying them to an actual soil profile at different return periods in different seismic environments. The methodology was used to illustrate differences between performance-based and conventional evaluation of liquefaction potential. These analyses led to the following conclusions:

1. The actual potential for liquefaction, considering all levels of ground motion, is influenced by the position and slope of the peak acceleration hazard curve and by the distributions of earthquake magnitude that contribute to peak acceleration hazard at different return periods.

2. Consistent application of conventional procedures for evaluation of liquefaction potential (i.e. based on a single ground motion level) to sites in different seismic environments can produce highly inconsistent estimates of actual liquefaction hazards.
3. Criteria based on conventional procedures for evaluation of liquefaction potential can produce significantly different liquefaction hazards even for sites in relatively close proximity to each other. For the locations considered in this paper, such criteria were generally more strict (i.e. resulted in longer return periods, hence lower probabilities, of liquefaction) for locations with flatter peak acceleration hazard curves than for locations with steeper hazard curves, and for locations at which large magnitude earthquakes contributed a relatively large proportion of the total hazard.
4. Criteria that would produce more uniform liquefaction hazards at locations in all seismic environments could be developed by specifying a standard return period for liquefaction. Performance-based procedures such as the one described in this paper could be used to evaluate individual sites with respect to such criteria.
5. The use of a "capacity-related" parameter, such as required SPT resistance, can be useful for liquefaction potential evaluation. The required penetration resistance is independent of the insitu penetration resistance and therefore exhibits smooth and gradual spatial variation that leads to smoother contours when mapped for a given hazard level.
6. A performance-based value of required penetration resistance, i.e., a value that reflects the contributions of all peak accelerations and magnitudes contributing to ground shaking hazards and the uncertainty in liquefaction resistance, can be computed and mapped by a person familiar with the performance-based liquefaction potential evaluation process.
7. The relatively consistent and smoothly varying ratio of total to effective vertical stress and depth reduction factor in typical liquefiable profiles, along with the relative insensitivity of the depth reduction factor to peak acceleration and magnitude, allow required penetration resistances at different depths in a soil profile to be related to each other in a predictable manner.
8. The basic equations on which available probabilistic liquefaction potential evaluation procedures are based can be manipulated to establish well-grounded adjustment factors that relate required penetration resistances and factors of safety for a reference profile to those for a site-specific profile.
9. Testing of the adjustment procedures at different depths, return periods, and seismic environments shows very good agreement with required penetration resistances and factors of safety directly computed from complete performance-based liquefaction potential analyses.
10. The proposed adjustment procedures produce results that can be somewhat conservative for locations whose seismicity is dominated by very large, historical earthquakes. For such locations, complete performance-based liquefaction potential analyses are recommended.
11. The procedures described in this paper provide a reasonable approximation to a complete, performance-based liquefaction potential evaluation without requiring the user to perform

the performance-based calculations. Using a mapped value of required penetration resistance that was obtained by a complete, performance-based analysis, the engineer needs only to compute three adjustment factors using deterministic, algebraic equations.

References

Arango, I., Ostadan, F, Cameron, J., Wu, C.L., and Chang, C.Y. (2004). "Liquefaction probability of the BART Transbay Tube backfill," Proceedings of the 11th International Conference on Soil Dynamics and Earthquake Engineering and 3rd International Conference on Earthquake Geotechnical Engineering, Vol. I, pp. 456-462.

Atkinson, G.M., Finn, W.D.L., and Charlwood, R.G. (1984). "Simple computation of liquefaction probability for seismic hazard applications," *Earthquake Spectra,* 1(1), 107-123.

Baker J.W. and Faber M. (2008). "Liquefaction risk assessment using geostatistics to account for soil spatial variability," *Journal of Geotechnical and Geoenvironmental Engineering,* ASCE, 134 (1), 14-23.

Cetin, K.O. (2000). "Reliability-based assessment of seismic soil liquefaction initiation hazard," Ph.D. Dissertation, University of California, Berkeley, 602 pp.

Cetin, K.O., Der Kiureghian, A., and Seed, R.B. (2002). "Probabilistic models for the initiation of seismic soil liquefaction," Structural Safety, 24(1), 67-82.

Cetin, K.O., Seed, R.B., Der Kiureghian, A., Tokimatsu, K., Harder, L.F., Kayen, R.E., and Moss, R.E.S. (2004). "Standard penetration test-based probabilistic and deterministic assessment of seismic soil liquefaction potential," *Journal of Geotechnical and Geoenvironmental Engineering*, ASCE, 130(12), 1314-1340.

Cornell, C.A. (1968). "Engineering seismic risk analysis," *Bulletin of the Seismological Society of America,* 58(5), 1583-1606.

Cornell, C.A. and Krawinkler, H. (2000). "Progress and challenges in seismic performance assessment," *PEER News*, April, 1-3.

Deierlein, G.G., Krawinkler, H., and Cornell, C.A. (2003). "A framework for performance-based earthquake engineering," Proceedings, 2003 Pacific Conference on Earthquake Engineering.

Hwang, J.H., Chen, C.H., and Juang, C.H. (2005). "Liquefaction hazard: a fully probabilistic method," in *Proceedings of the Sessions of the Geo-Frontiers 2005 Congress,* Earthquake Engineering and Soil Dynamics, R.W. Boulanger et al. eds, ASCE, Paper no. 22.

Idriss, I.M. and Boulanger, R.W. (2004). "Semi empirical procedures for evaluating liquefaction potential during earthquakes," *Proceedings of the 11th International Conference on Soil Dynamics and Earthquake Engineering and 3rd International Conference on Earthquake Geotechnical Engineering,* Vol. I, 32-56.

Juang, C.H. and Jiang, T. (2000). "Assessing probabilistic methods for liquefaction potential evaluation," *Soil Dynamics and Liquefaction*, Geotechnical Special Publication No. 107, R.Y.S. Pak and J. Yamamura, eds., ASCE, Reston, VA, pp. 148-162, 2000.

Kayen, R. E., and Mitchell, J. K. (1997). "Assessment of liquefaction potential during earthquakes by Arias intensity," *Journal of Geotechnical and Geoenvironmental Engineering.* 123(12), 1162–1174.

Kramer, S.L. and Mayfield, R.T. (2005). "Performance-based liquefaction hazard evaluation," in *Proceedings of the Sessions of the Geo-Frontiers 2005 Congress,* Earthquake Engineering and Soil Dynamics, R.W. Boulanger et al. eds, ASCE, Paper no. 21.

Kramer, S.L. and Mayfield, R.T. (2007). "Return period of soil liquefaction," *Journal of Geotechnical and Geoenvironmental Engineering*, ASCE, 133(7), 802-813.

Kramer, S.L. and Mitchell, R.A. (2006). "Ground motion intensity measures for liquefaction hazard evaluation," *Earthquake Spectra*, 22(2), 413-438.

Krawinkler, H. (2002). "A general approach to seismic performance assessment," *Proceedings*, International Conference on Advances and New Challenges in Earthquake Engineering Research, ICANCEER, 2002, Hong Kong.

Leyendecker, E.V., Hunt, R.J., Frankel, A.D., and Rukstales, K.R. (2000). "Development of maximum considered earthquake ground motion maps," *Earthquake Spectra*, 16(1), 21-40.

Liao, S.S.C., Veneziano, D., and Whitman, R.V. (1988). "Regression models for evaluating liquefaction probability," *Journal of Geotechnical Engineering,* ASCE, 114(4), 389-409.

Marrone, J., Ostadan, F., Youngs, R., and Litehiser, J. (2003). “Probabilistic liquefaction hazard evaluation: method and application,” in *Transactions of the 17th International Conference on Structural Mechanics in Reactor Technology (SMiRT 17)*, Prague, Czech Republic, Paper no. M02-1.

Martin, G.R. and Lew, M. eds. (1999). “Recommended Procedures for Implementation of DMG Special Publication 117 – Guidelines for Analyzing and Mitigating Liquefaction Hazards in California,” Southern California Earthquake Center, Los Angeles, 63 pp.

McGuire, R.K. (1995). “Probabilistic seismic hazard analysis and design earthquakes: Closing the loop,” *Bulletin of the Seismological Society of America*, 85(5), 1275-1284.

National Center for Earthquake Engineering Research (1997). *Proceedings of the NCEER workshop on evaluation of liquefaction resistance of soils*, T.L. Youd and I.M. Idriss, editors, Technical Report NCEER, 97-022.

Seed, H. B and Idriss, I. M _1983_. *Ground motions and soil liquefaction during earthquakes*, Earthquake Engineering Research Institute, Berkeley, Calif., 134 pp.

Seed, H.B. and Idriss, I.M. (1971). "Simplified procedure for evaluating soil liquefaction potential," *Journal of the Soil Mechanics and Foundations Division* , ASCE, 107(SM9), 1249-1274.

Seed, H.B., Tokimatsu, K., Harder, L.F., and Chung, R.M. (1985). "Influence of SPT procedures in soil liquefaction resistance evaluations," *Journal of Geotechnical Engineering*, 111(12), 1425-1445.

Stewart, J.P., Liu, A.H., and Choi, Y. (2003). Amplification factors for spectral acceleration in tectonically active regions,” *Bulletin of the Seismological Society of America*, 93(1), 332-352.

Toprak, S., Holzer, T.L., Bennett, M.J., and Tinsley, J.C. III. (1999). “CPT- and SPT-based probabilistic assessment of liquefaction,” *Proc., 7th U.S.-Japan Workshop on Earthquake Resistant Design of Lifeline Facilities and Countermeasures Against Liquefaction*, Seattle, Multidisciplinary Center for Earthquake Engineering Research, Buffalo, NY, 69-86.

Toro, G.R., Abrahamson, N.A., and Schneider, J.F. (1997). “Model of strong ground motions from earthquakes in central and eastern North America: Best estimates and uncertainties,” *Seismological Research Letters*, 68(1), 41-57.

Yegian, M.Y. and Whitman, R.V. (1978). “Risk analysis for ground failure by liquefaction,” *Journal of the Geotechnical Engineering* Division, ASCE, 104(GT7), 907-905.

Youd, T.L. and Noble, S.K. (1997). “Liquefaction criteria based on statistical and probabilistic analyses,” *Proceedings of the NCEER Workshop on Evaluation of Liquefaction Resistance of Soils*, National Center for Earthquake Engineering Research, Buffalo, NY, 201-205.

Youd, T.L. et al. (2001). “Liquefaction resistance of soils: Summary report from the 1996 NCEER and 1998 NCEER/NSF workshops on evaluation of liquefaction resistance of soils,” *Journal of Geotechnical and Geoenvironmental Engineering*, ASCE, 127(10), 817-833.